JOURNAL OF GEOPHYSICAL RESEARCH, VOL. 105, NO. C5, PAGES 11,385–11,406, MAY 15, 2000

Characteristics of three-dimensional quasi-geostrophic transient eddy propagation in the vicinity of a simulated Gulf Stream

Mototaka Nakamura and Yi Chao

Jet Propulsion Laboratory, California Institute of Technology, Pasadena

Abstract. Output of an eddy-resolving model of the North Atlantic is diagnosed in the vicinity of the Gulf Stream (GS), using the three-dimensional quasi-geostrophic transient wave activity flux diagnostic developed by *Plumb* [1986]. The model North Atlantic shows large transient wave activity along the model GS and along the edge of the Mediterranean Outflow. The fluxes show advection of wave activity by the GS from the separation point and radiation of wave activity from the GS in the top 1000 m. The wave radiation from the model GS is particularly clear to its south and points southwestward in general. The fluxes in and around the Mediterranean Outflow appear to be generated and dissipated locally. The vertical component of the transient wave activity flux is downward on average at all depths, suggesting conversion of baroclinic energy supplied near the surface into kinetic energy distributed throughout the depth. Eddy fields show that transient eddies tend to reinforce quasi-stationary meanders in the GS just downstream of the separation point. We also find evidence for eddy forcing of the northern recirculation generated in the model, in agreement with the available observations.

1. Introduction

Mesoscale eddies are particularly energetic in the vicinity of the Gulf Stream (GS) and the North Atlantic Current (NAC). Eddy kinetic energy along these currents is estimated to be several orders of magnitude greater than that in the surrounding quiet regions [e.g., *Wyrtki et al*., 1976; *Schmitz et al*., 1983; *Krauss*, 1986]. It has been speculated that the GS is the source of eddy activity for far fields through wave radiation [*Wunsch*, 1983; *Schmitz et al*., 1983]. Although steadily propagating disturbances toward the east cannot radiate energy into Rossby wave motions [*Pedlosky*, 1977], disturbances supported by a basic state jet that has some meridional component can radiate energy into far fields effectively [*Kamenkovich and Pedlosky*, 1996, 1998]. Also, transience of propagating disturbances, such as growth and decay of meanders observed along the GS, can radiate wave energy [*Malanotte-Rizzoli et al*., 1987]. *Hogg* [1988] and *Malanotte-Rizzoli et al*. [1995] demonstrated that such transience of the GS meanders can radiate wave energy away into far fields and induce circulations away from the GS. Recirculations observed to the north and south of the GS may be driven by the wave energy radiated away from the GS [*Hogg*, 1988; *Malanotte-Rizzoli et al*., 1995]. Indeed, such eddy-driven recirculation cells are observed in idealized model experiments [e.g., *Holland and Rhines*, 1980]. On the other hand, stability analysis and studies with an idealized model by *Spall* [1994] suggest that open ocean baroclinic instability can generate mesoscale eddies in the interior of the oceans away from the GS.

Observational evidence of wave radiation from the GS is limited because of the limited data available for calculations of second-order statistics of oceanic motions with a reasonably accuracy. However, *Bower and Hogg* [1992] found evidence of barotropic wave radiation from the GS in the deep ocean to the north of the GS from available current meter data. Also, *Chester et al*. [1994] analyzed the Synoptic Ocean Prediction (SYNOP) tomographic data using a simplified version of the three-dimensional transient wave activity flux diagnostic developed by *Plumb* [1986]. They computed the wave activity flux at 500 and 1000 m depths and found evidence of southward and downward radiation of transient waves from the GS in the vicinity of 55°W and 37°N.

Potentially important roles that mesoscale eddies may play in forcing and maintaining large-scale circulations have been studied by theories [*Rhines and Holland*, 1979; *Rhines and Young*, 1982a, b] and idealized models [e.g., *Holland*, 1978; *Holland and Rhines*, 1980]. These theoretical and model studies suggested very important roles of transient eddies in driving large-scale circulations in the presence of large-scale wind forcing that provides energy to the eddies. An observational effort in describing the role of eddies in large-scale circulations also suggests that transient eddies play an important role in driving the mean frontal current of the GS by pumping momentum into the mean flow jet [*Schmitz et al*., 1983]. Also, a similar pattern of eddy momentum forcing of the mean subtropical jet in the atmosphere is well known [e.g., *Oort and Peixoto*, 1983]. Because of their likely important roles in driving the mean flow and in transport and mixing of heat and salt in regions that are particularly important in forcing the midlatitude atmosphere, mesoscale eddies may play critical roles in maintenance and fluctuations of regional and global climates as well. Therefore understanding the roles of these eddies in the large-scale oceanic circulations may be crucial to understanding the dynamics of climate.

Here we have attempted to study characteristics of generation, propagation, and dissipation (or absorption) of wave activity in the North Atlantic, focusing on the vicinity of the GS and the NAC. Because of the lack of sufficient data to perform

Paper number 2000JC900013.
0148-0227/00/2000JC900013$09.00

such a study, we have used output of an eddy-resolving model of the North Atlantic as pseudodata. Although the models are not perfect and lack certain physics, the output of such models is dynamically consistent and available at regular intervals in space and time. If the model reproduces some key observed features reasonably well, the diagnostic results may well reflect some of the reality. Results may well suggest to us what parts of the oceans are more likely to provide us with key information in studying various facets of the oceanic flows and thus help us target the observational efforts more effectively. Also, application of diagnostic tools to model output may be used as a means to diagnose problems in the model solutions and thus may provide useful information for future improvements of the model. Section 2 briefly describes the model output used for the study. Section 3 describes the formulation of *Plumb*'s [1986] three-dimensional transient wave activity flux diagnostic and minor modifications made for the current study. Section 4 describes and discusses the diagnosed transient wave activity and its fluxes. Section 5 discusses diagnoses of the eddy time mean relationship in large-amplitude meanders in the model GS. Section 6 describes the eddy fields at 55°W in relation to the model's northern and southern recirculations. Finally, section 7 summarizes and discusses the results.

2. Pseudodata

The pseudodata used for the calculations are from a 30 year integration of an eddy-resolving general circulation model (GCM) of the North Atlantic described by *Chao et al*. [1996]. The model is based on the Parallel Ocean Program (POP) developed at Los Alamos National Laboratory [*Dukowicz and Smith*, 1994]. The POP is a free surface version of the primitive equation model developed at the Geophysical Fluid Dynamics Laboratory [*Bryan*, 1969; *Cox*, 1984]. The model basin covers the Atlantic basin from 35°S to 80°N and from 100°W to 20°E. The horizontal grid spacing of the model is ~1/6° (0.1875° in longitude and 0.1843° in latitude). There are unevenly spaced 37 vertical levels in the model. There are 19 levels in the top 1000 m, with the thickness of each model layer varying from 11 m at the surface to 198 m at 901 m. Below the top 1000 m all levels have the same thickness, 250 m. At artificial boundaries of the model ocean, temperature and salinity are restored toward seasonal climatology. The portion of integration from which we extract the output is driven with the surface salinity restored toward the Levitus climatology [*Levitus et al*., 1994], the surface heat flux derived from the European Centre for Medium-Range Weather Forecast (ECMWF) analysis, and the surface wind stress derived from the ECMWF analysis. The reader is referred to *Chao et al*. [1996] for more details of the model integration and simulation results. As described by *Chao et al*. [1996], the model has reproduced some of the observed characteristics of the GS reasonably well. In particular, the separation point and the mean path of the GS are reproduced reasonably well. The model GS does, however, show unrealistic features. In particular, the model GS has significantly stronger quasi-stationary meanders along its path downstream of the separation point than does the observed. Also, the model GS underestimates kinetic energy considerably compared to some observational values at depth [*Owens*, 1991; *Richardson*, 1993]. Also, farther downstream, the characteristic 90° northward turn of the current toward the Northwest Corner is not reproduced well in the model. Rather than turning northward, the current becomes split, producing some flow turning north and some flow shooting toward northeast. This problem has been observed in other North Atlantic Ocean simulations by eddy-resolving models [e.g., *Bryan and Holland*, 1989; *Semtner and Chervin*, 1992; *Smith et al*., 1992; *Beckmann et al*., 1994].

We focus our attention on a domain that covers 30°–60°N and 75°–15°W for the present work. The choice is made to cover most of the GS after separation from the western boundary and the NAC and to make calculations of the diagnostics reasonably efficient on our computational resources. The three-dimensional model output is saved every 3 days. This sampling frequency is sufficient to obtain smooth evolution of temperature and salinity fields, as well as the velocity field, from the saved output. However, the output contains fluctuations of very high frequency that are likely to produce strong noise in the diagnostic results. Time series of 3 day mean fields, instead of snap shots at a 3 day interval, may well reduce the noise significantly. Because of the lack of computer memory for storing such 3 day mean fields during the model integration, we do not have an option of using the 3 day mean fields for the calculations to be presented. The portion of the model output employed for the diagnostics is from March of year 25 to February of year 30. During this 5 year period, 600 snapshots of potential temperature, salinity, and horizontal velocity are available. From the temperature and salinity output we compute in situ density and potential density using the full nonlinear equation of state used in the model integration. Local stratification is used for computation of quasi-geostrophic potential vorticity.

3. Formulation of Three-Dimensional Quasi-geostrophic Transient Wave Activity Flux

Plumb [1986] derived an expression for an approximate conservation equation for transient wave activity using a quasi-geostrophic eddy enstrophy equation of a form,

$$\frac{d\eta}{dt} + \overline{\mathbf{v}'q'} \cdot \nabla_{\mathbf{h}} \bar{q} = \overline{s'q'}, \tag{1}$$

where d/dt is the derivative following the geostrophic flow and s represents the sink or source of quasi-geostrophic potential vorticity, q. A subscript $\mathbf{h}$ denotes a horizontal vector. An overbar denotes the time average, and a prime denotes a deviation from the average. Here eddy potential enstrophy η is defined by

$$\eta = \frac{\overline{q'^2}}{2}, \tag{2}$$

where q is defined by

$$q = f + \frac{1}{a^2 \cos^2 \phi} \frac{\partial^2 \psi}{\partial \lambda^2} + \frac{1}{a^2 \cos^2 \phi} \frac{\partial}{\partial \phi} \left(\cos \phi \frac{\partial \psi}{\partial \phi} \right) + \frac{\partial}{\partial z} \left(\frac{f^2}{N^2} \frac{\partial \psi}{\partial z} \right) \approx f + \zeta + \frac{\partial}{\partial z} \left(\frac{f^2}{N^2} \frac{\partial \psi}{\partial z} \right). \tag{3}$$

Here λ and ϕ are longitude and latitude, respectively, a is the radius of the Earth, f is the planetary vorticity, ζ is relative vorticity, ψ is the stream function, and N^2 is the Brunt-Väisälä frequency. The triple correlation term $\overline{\mathbf{v}'q'} \cdot \overline{\nabla_{\mathbf{h}} q'}$ has been neglected with respect to $\overline{\mathbf{v}'q'} \cdot \nabla_{\mathbf{h}} \bar{q}$ in (1). *Plumb* [1986] notes that the triple correlation term may be absorbed into the right-hand side of (1), making the right-hand side term a combina-

tion of source/sink and nonlinear effects. We have found that the triple correlation term is not negligible in general in the pseudodata used for the current study (M. Nakamura and Y. Chao, Diagnoses of an eddy-resolving Atlantic Ocean model simulation in the vicinity of the Gulf Stream, II, Eddy potential enstrophy and eddy potential vorticity fluxes, submitted to *Journal of Physical Oceanography*, 1999b, hereinafter referred to as Nakamura and Chao, submitted manuscript, 1999b) and thus consider the right-hand side of (1) to be a combination of source/sink and nonlinear effects. With two simplifying assumptions, *Plumb* [1986] showed that (1) can be manipulated to yield a conservation equation for quasi-geostrophic wave activity M,

$$\frac{\partial M}{\partial t} + \nabla \cdot \mathbf{M_T} = S_M, \tag{4}$$

where

$$S_M = \frac{\overline{s'q'}\cos\phi}{|\nabla_{\mathbf{h}}\bar{q}|}, \tag{5}$$

$$M = \frac{\eta\cos\phi}{|\nabla_{\mathbf{h}}\bar{q}|}, \tag{6}$$

and the total wave activity flux $\mathbf{M_T}$ is given by the sum of the radiative wave activity flux and the advective flux

$$\mathbf{M_T} = \mathbf{M_R} + \bar{\mathbf{V}}_{\mathbf{h}}M. \tag{7}$$

The radiative flux $\mathbf{M_R}$ is defined by

$$M_{Ri} = n_j B_{j,i}, \tag{8}$$

where $\mathbf{n}$ and $\mathbf{B}$ are defined by

$$\mathbf{n} = \frac{\nabla_h\bar{q}}{|\nabla_{\mathbf{h}}\bar{q}|} \tag{9}$$

$$\mathbf{B} = \cos\phi \cdot \begin{bmatrix} -\dfrac{1}{a^2\cos^2\phi}\overline{\dfrac{\partial\psi'}{\partial\lambda}\dfrac{\partial\psi'}{\partial\phi}} & \varepsilon - \dfrac{1}{a^2}\overline{\left(\dfrac{\partial\psi'}{\partial\phi}\right)^2} & \dfrac{-f^2}{aN^2}\overline{\dfrac{\partial\psi'}{\partial\phi}\dfrac{\partial\psi'}{\partial z}} \\ \dfrac{1}{a^2\cos^2\phi}\overline{\left(\dfrac{\partial\psi'}{\partial\lambda}\right)^2} - \varepsilon & \dfrac{1}{a^2\cos^2\phi}\overline{\dfrac{\partial\psi'}{\partial\lambda}\dfrac{\partial\psi'}{\partial\phi}} & \dfrac{-f^2}{aN^2\cos\phi}\overline{\dfrac{\partial\psi'}{\partial\lambda}\dfrac{\partial\psi'}{\partial z}} \\ 0 & 0 & 0 \end{bmatrix},$$

where

$$\varepsilon = \frac{1}{2}\left[\frac{1}{a^2\cos^2\phi}\overline{\left(\frac{\partial\psi'}{\partial\lambda}\right)^2} + \frac{1}{a^2}\overline{\left(\frac{\partial\psi'}{\partial\phi}\right)^2} + \frac{f^2}{N^2}\overline{\left(\frac{\partial\psi'}{\partial z}\right)^2}\right]. \tag{10}$$

The two simplifying assumptions necessary to derive the conservation equation, (4), are (1) the $\bar{q}$ gradient is slowly varying in the direction of the mean flow as compared to the eddy enstrophy and (2) the direction of the $\bar{q}$ gradient is slowly varying compared to $\mathbf{B}$. The radiative component $\mathbf{M_R}$ is essentially a generalization of the Eliassen-Palm flux [*Eliassen and Palm*, 1961] for the time mean flow with zonal variations. Also, *Plumb* [1985] showed that in the almost plane wave limit, $\mathbf{M_T}$ is everywhere parallel to the group velocity of transient waves. It thus provides us with information on the mean direction of propagation of transient waves and the energy associated with them in this limit. It is clear from (4)–(10) that the magnitude of $\mathbf{M_T}$ indicates the strength of transient waves and that the convergence of $\mathbf{M_T}$ is related to nonconservative effects that suggest dissipation or absorption of the wave activity and vice versa.

We have used *Plumb*'s [1986] formula given by (4)–(10) with only slight modifications for our calculations. We compute q by

$$q = f + \zeta + f\frac{\dfrac{\partial\sigma^*}{\partial z}}{\dfrac{d\sigma_0}{dz}}, \tag{11}$$

where σ_0 is the reference potential density, which is a function of depth only, and σ^* is the deviation in σ from σ_0. The last term on the right-hand side of (11) may be approximated by $-(\partial/\partial z)(fg\sigma^*/\rho_0 N^2)$, where ρ_0 is the reference density at a constant depth. Thus we replace $f^2/N^2\ \partial\psi'/\partial z$ with $-(fg\sigma^{*\prime}/N^2\rho_0)$. Also, as by *Plumb* [1986], we assume $u \approx -1/a\ \partial\psi/\partial\phi$ and $v \approx 1/(a\cos\phi)\ \partial\psi/\partial\lambda$. With these approximations we obtain

$$\mathbf{M_R} = M_R^x\hat{\mathbf{i}} + M_R^y\hat{\mathbf{j}} + M_R^z\hat{\mathbf{k}}, \tag{12}$$

where

$$M_R^x = \frac{\cos\phi}{|\nabla_h\bar{q}|}\left[\frac{\partial\bar{q}}{\partial x}\overline{u'v'} + \frac{\partial\bar{q}}{\partial y}(\overline{v'^2} - \varepsilon)\right], \tag{13}$$

$$M_R^y = \frac{\cos\phi}{|\nabla_h\bar{q}|}\left[\frac{\partial\bar{q}}{\partial x}(\varepsilon - \overline{u'^2}) - \frac{\partial\bar{q}}{\partial y}\overline{u'v'}\right], \tag{14}$$

$$M_R^z = \frac{f\cos\phi}{|\nabla_h\bar{q}|\dfrac{d\bar{\sigma}_0}{dz}}\left(\frac{\partial\bar{q}}{\partial x}\overline{u'\sigma^{*\prime}} + \frac{\partial\bar{q}}{\partial y}\overline{v'\sigma^{*\prime}}\right), \tag{15}$$

$$\varepsilon = \frac{1}{2}\left(\overline{u'^2} + \overline{v'^2} - \frac{g}{\bar{\sigma}_0}\frac{\overline{\sigma^{*\prime 2}}}{\dfrac{d\bar{\sigma}_0}{dz}}\right). \tag{16}$$

Our formula reduces to that used by *Chester et al*. [1994] when $\partial\bar{q}/\partial x$ is much smaller than $\partial\bar{q}/\partial y$ and potential density perturbations are dominated by potential temperature perturbations. We emphasize that assumptions of small-amplitude perturbations, slowly varying $|\nabla_{\mathbf{h}}\bar{q}|$ in the direction of the mean flow as compared with the eddy enstrophy, and slowly varying direction of $\nabla_{\mathbf{h}}\bar{q}$ as compared to $\mathbf{B}$ may not be as well justified in our case as they are in atmospheric cases examined by *Plumb* [1986]. We have found that large-amplitude eddies play critical roles in formation of the mean structures in the domain considered here. Also, there are small-scale structures in $\bar{q}$ that have the same scale as those of eddy correlation terms. Therefore the reader must keep in mind the limitation of the diagnostic approach and should interpret the results with caution. With an objective of estimating the first-order linear propagation characteristics of quasi-geostrophic eddies in this domain we compute the three-dimensional transient wave activity flux, applying (4)–(16) to the 5 year model output described in section 2. To reduce noisy structures in the time mean fields, we smooth them by applying a nine-point equal weight averaging to the time mean. Eddies are calculated by subtracting the smoothed time mean field from the total field for each variable. We have not attempted to filter out the seasonal cycle since such filtering shall result in some loss of true wave signals. Therefore the wave activity and fluxes of the wave activity do contain effects of the seasonal cycle. Below the mixed layer the effect of the seasonal cycle weakens considerably, allowing a

straight interpretation of the wave activity as that due to quasi-geostrophic transient waves.

4. Wave Activity and Wave Activity Fluxes

4.1. Wave Activity

Transient wave activity M as defined by (6) is essentially a measure of transient eddy amplitudes at a given location. It arises mainly from three different sources in the model. Obvious sources are transient motions associated with baroclinic and barotropic waves. These motions are expected to be strong along the GS. Another possible source is transient motions generated by flows associated with waves induced by topography. This may be a significant source of M where strong flows are observed along lateral boundaries or on sloping bottoms, including bottom topography. (The model ocean is assumed to be in a hydrostatic balance, and therefore internal gravity waves are not represented by the wave activity fluxes.) The horizontal and vertical structures of M show large spatial variations in the wave activity in the model ocean. Plate 1 shows $\log_{10}$ of M at selected levels. Because of the relatively short time series used for the diagnoses, M is noisy. However, gross large-scale horizontal structures can be seen fairly clearly. In general, M is large near the surface and small at deeper levels, with a very large range of the order of magnitude from 10^{-5} to 10^{3} m s^{-1}. Even at a given level, a range of the order of magnitude of M is very large, typically 5 orders of magnitude at each level. There are two regions that show large values (with respect to other regions at a given depth) in M. One is a band near the edge of the Mediterranean Outflow, and the other is the vicinity of the GS. (The model Mediterranean Outflow is somewhat displaced from the observed position.) In both regions the maximum values occur near the surface with a slight difference in the depth at which the maximum occurs. In the vicinity of the GS, quite large values are observed between 100 and 1000 m (Plate 1b), while only the top 50 m shows very large values over the edge of the Mediterranean Outflow (Plate 1a). As shown in the following section, $\bar{\mathbf{V}}_{\mathbf{h}}M$ is large along the model GS, generally decreasing downstream from the separation point. On the other hand, it will be shown that $\bar{\mathbf{V}}_{\mathbf{h}}M$ originates from and converges in the region of large M in the top 50 m over the edge of the Mediterranean Outflow. These features imply that the large M over the edge of the Mediterranean Outflow is entirely locally generated, most likely by baroclinic instability such as that discussed by *Spall* [1994], while the large M along the GS is due to both the mean flow advection of M and the local generation by baroclinic and barotropic instabilities.

Below the near-surface maximum, M shows very small values at middepths in these two regions. The layer of very small M in these regions lies above a layer of fairly large M, creating middepth minima. Plate 2 shows a vertical cross section of $\log_{10}$ of M, averaged from 37.5° to 42.5°W. Points where the average is computed from a longitudinal band with a width <2° because of topography are treated as land points in Plate 2. As is evident in Plate 2, there are layers of small (order 10^{-1} m s^{-1}) M below the model GS (38°–50°N) above 2500 m and below the band of very large M near the surface (32°–38°N) between 200 and 400 m. Inspections of cross sections at other longitudes show that the latter shallow local minimum below the band of very large M near the surface is observed clearly only over the bottom topography associated with the Mid-Atlantic Ridge (MAR). These local minima in M at different depths suggest that baroclinic waves may have substantially different vertical structures in these two regions, perhaps controlled by the bottom topography.

4.2. Horizontal Fluxes

Horizontal fluxes of transient wave activity M consist of the mean flow advection of the wave activity, $\bar{\mathbf{V}}_{\mathbf{h}}M$, and radiation of the wave activity, $\mathbf{M}_{\mathbf{Rh}}$. Plate 3 shows the horizontal component of the total wave activity flux, $\mathbf{M}_{\mathbf{Th}}$, and the horizontal mean flow $\bar{\mathbf{V}}_{\mathbf{h}}$ superimposed on $\bar{q}$ at selected levels of the model. (Structures of $\bar{q}$ are described and discussed in detail by M. Nakamura and Y. Chao (Diagnoses of an eddy-resolving Atlantic Ocean model simulation in the vicinity of the Gulf Stream, I, Potential vorticity, submitted to *Journal of Physical Oceanography*, 1999a).)

The most striking features in $\mathbf{M}_{\mathbf{Th}}$ are the advection of M by the GS from the vicinity of the separation point and the radiation of M from the GS along its path in the top 1000 m (Plates 3a, 3b, and 3c). Inspections of $\bar{\mathbf{V}}_{\mathbf{h}}M$ and $\mathbf{M}_{\mathbf{Rh}}$ show that $\bar{\mathbf{V}}_{\mathbf{h}}M$ advects M from the separation point along the GS path, gradually decreasing downstream, although $\bar{\mathbf{V}}_{\mathbf{h}}M$ shows some local convergence and divergence along the path. In the top 500 m, $\mathbf{M}_{\mathbf{Th}}$ consists almost entirely of $\bar{\mathbf{V}}_{\mathbf{h}}M$ along the GS. The advective fluxes are particularly large in the top few hundred meters, where the model GS shows fairly realistic strength, and appear parallel to the contours of $\bar{q}$ to the lowest order. (The large fluxes in the region of large $\bar{q}$ in the top 50 m contain strong signals of the seasonal cycle and may not necessarily represent propagation of quasi-geostrophic waves at this level. However, we do observe active waves in this region in movies of q.) Below 500 m, $\bar{\mathbf{V}}_{\mathbf{h}}M$ by the model GS and $\mathbf{M}_{\mathbf{Rh}}$ have comparable magnitudes and tend to have the same direction to the north of the center of a tongue of high $\bar{q}$.

Inspections of $\mathbf{M}_{\mathbf{Rh}}$ show that the model GS radiates waves along its path, particularly clearly to its south toward south or southwest, in general, throughout the top 1000 m. Because of the small magnitude of $\mathbf{M}_{\mathbf{Rh}}$ to the south of the model GS, this is not visible in Plate 3. Plate 4 shows $\log_{10}(|\mathbf{M}_{\mathbf{Th}}|)\mathbf{m}$ at 577 and 1375 m, where $\mathbf{m}$ is a unit vector parallel to $\mathbf{M}_{\mathbf{Th}}$, to show weaker wave radiation more clearly. Much of the flux to the south of the GS appears to originate from either the main flow or the weaker southern branch of the model GS and becomes slightly larger toward the direction of propagation (Plate 4a). The fluxes are nearly parallel to the contours of $\bar{q}$ everywhere, even where $\mathbf{M}_{\mathbf{Rh}}$ dominates $\mathbf{M}_{\mathbf{Th}}$. (When wave energy density ε is dominated by eddy available potential energy, i.e.,

$$\varepsilon \approx -\frac{1}{2}\left(\frac{g}{\overline{\sigma_0}}\,\frac{\overline{\sigma^{*\prime 2}}}{\overline{\frac{d\sigma_0}{dz}}}\right),$$

it is easy to see that $(\nabla_{\mathbf{h}}\bar{q})\cdot\mathbf{M}_{\mathbf{Rh}} \approx 0$. It implies that transient eddies propagate along the contours of $\bar{q}$ to the lowest order when the mean flow is weak and the eddy available potential energy is much greater than the eddy kinetic energy.) The flux vectors suggest that the waves grow slightly as they propagate along the contours of $\bar{q}$ and exit the domain southward or southwestward near the southwestern corner of the domain in the top 400 m (not shown). At 577 m (Plate 4a), there is a clear sign of some fluxes returning to the vicinity of the separation point, suggesting that some of the wave activity radiated from the GS along its path is "recycled" and is fed back into the GS near the separation point. Wave activity converging into the

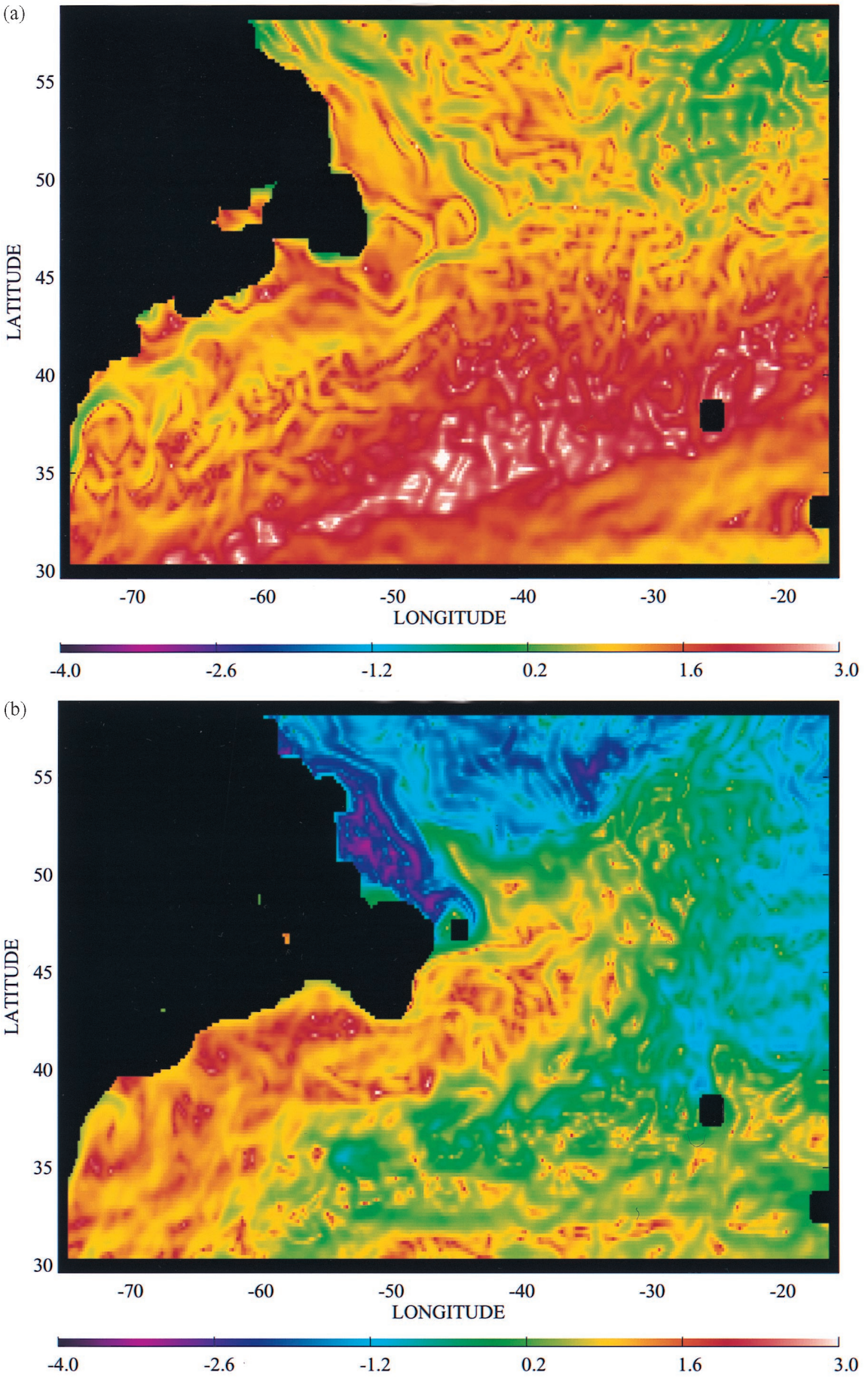

Plate 1. Horizontal plots of $\log_{10}$ of transient wave activity M at (a) 17, (b) 140, (c) 1375, and (d) 3375 m. Units of M are m s^{-1}.

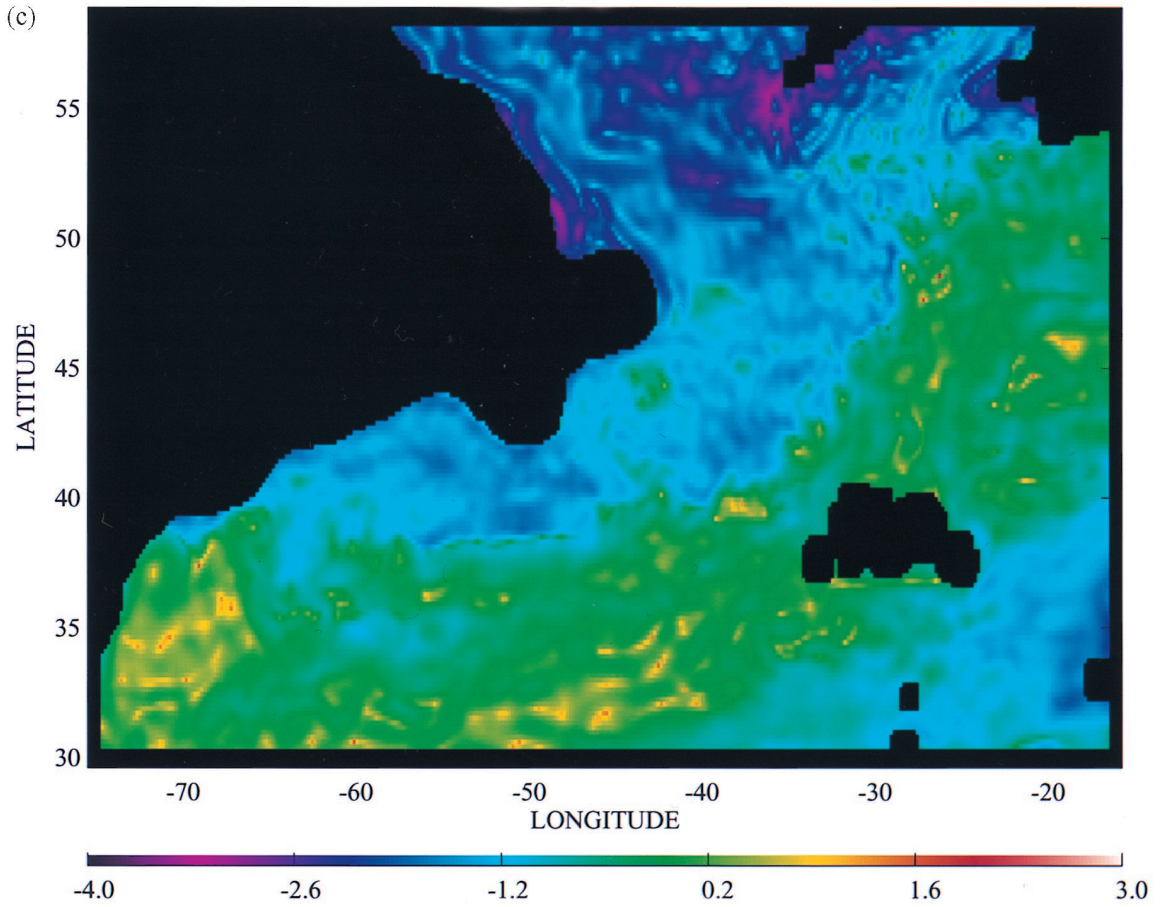

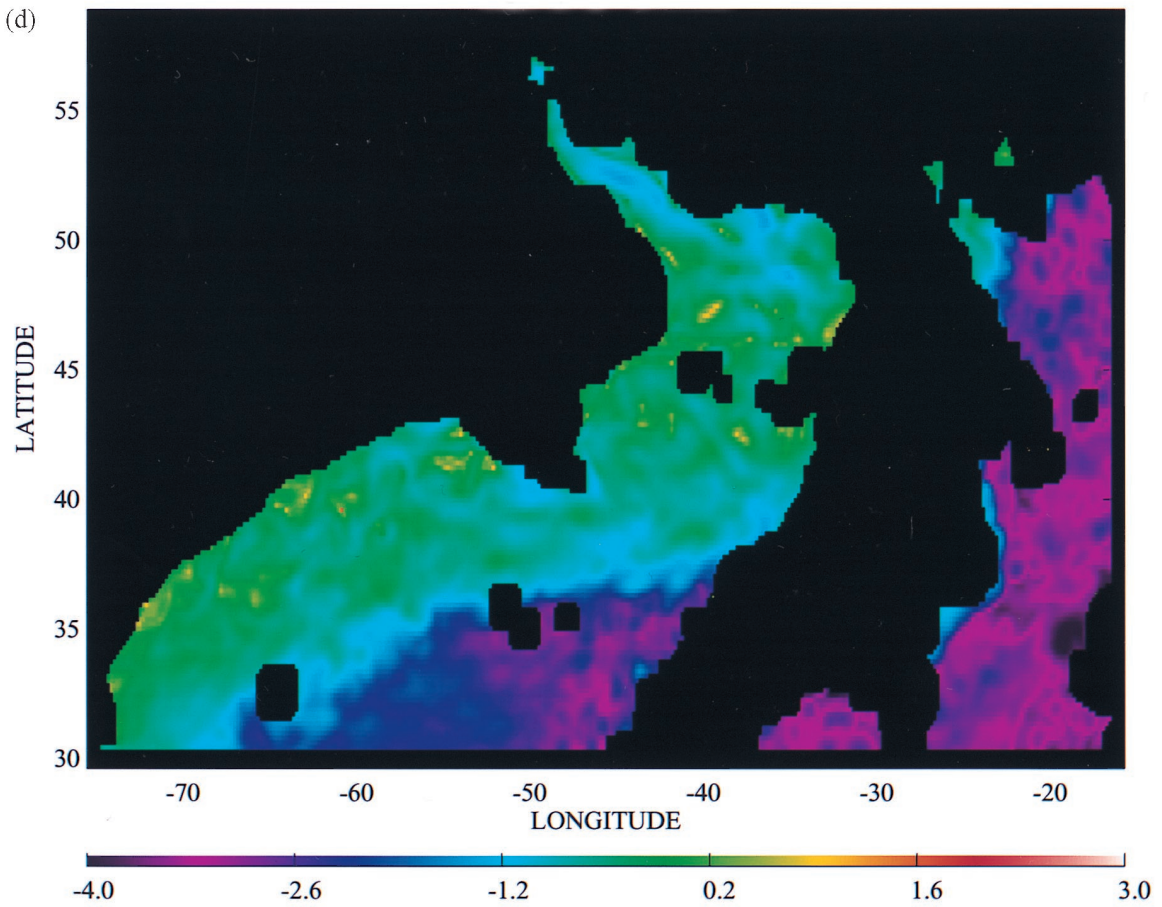

Plate 1. (continued)

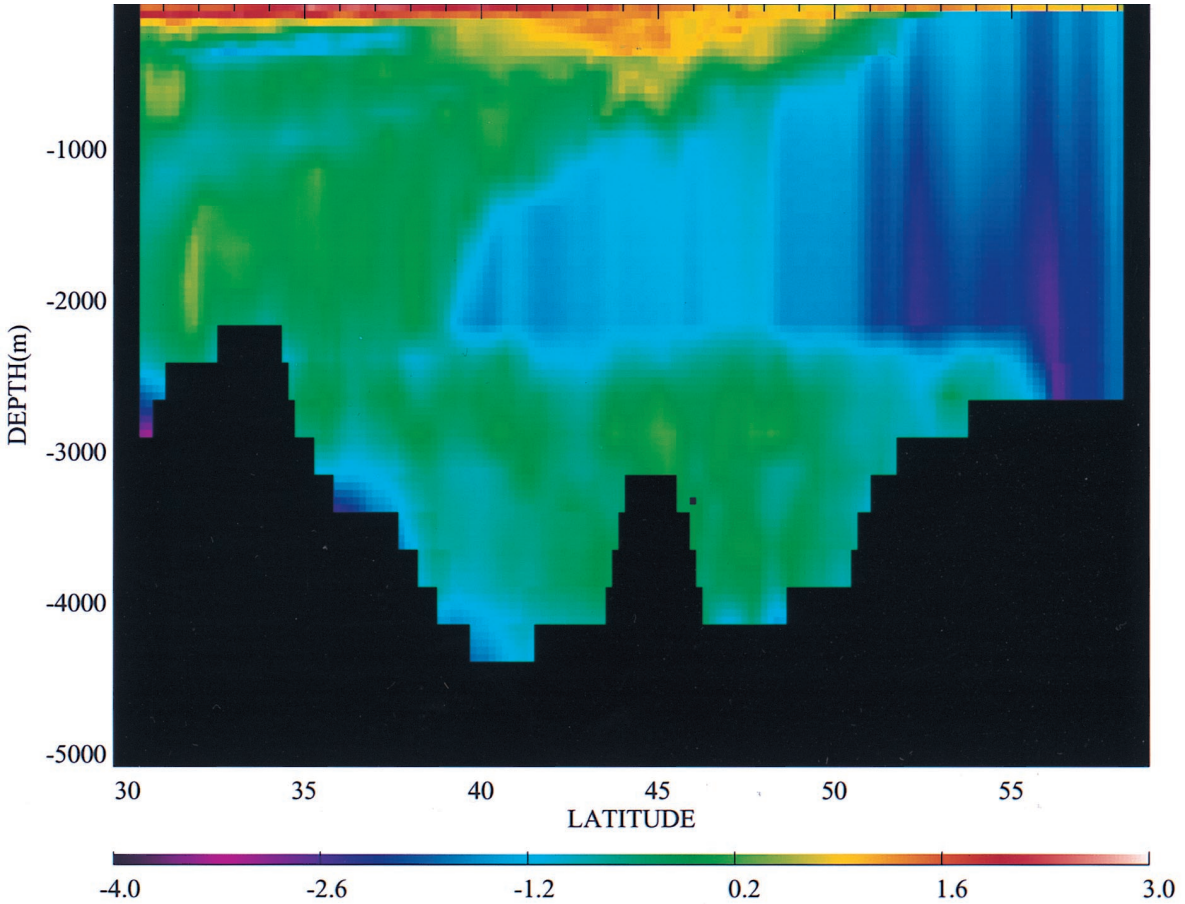

Plate 2. Vertical cross section of the 5° longitudinal average of $\log_{10}$ of M at 40°W. The vertical and horizontal coordinates are depth in meters and latitude in degrees, respectively. Units of M are m s^{-1}.

boundary region may be, in part, dissipating because of friction but may well be contributing to acceleration of the GS along the boundary or may simply be advected downstream by the GS. The southwestward or southward $\mathbf{M}_{\mathbf{Th}}$ exiting the domain of calculation at upper levels may be converging into the boundary region farther south outside of the domain also. Similar patterns of $\mathbf{M}_{\mathbf{Th}}$ are observed to the south of the center of the tongue of high $\bar{q}$ at 721 and 901 m levels, showing weaker recycling of wave activity in the vicinity of the GS. Wave radiation to the north of the model GS is not as clear as is that to the south of the GS, although $\mathbf{M}_{\mathbf{Rh}}$ is greater in magnitude to the north than it is to the south of the GS. However, as shown in an example in section 6, vertical cross sections of M_T^y show that there is also some northward wave radiation from the model GS.

These patterns of $\mathbf{M}_{\mathbf{Th}}$ in the vicinity of the GS in the top 1000 m suggest the following picture. The GS advects transient wave activity from a major source at the separation point (or farther upstream of the separation point, which is not covered in the current diagnosis) downstream along its path. As the wave activity is advected by the GS, it is also radiated from the GS. (The wave activity radiated from the GS is likely to contain wave activity that is locally generated in the vicinity of the GS by baroclinic and barotropic instabilities.) Some of this wave activity radiated from the GS is fed back into the GS in the vicinity of the separation point and farther upstream of the separation point, while some is dissipated at the boundary. The reader should note, however, that a slight displacement in the position of the model GS and the underestimated model GS and its eddy kinetic energy below the top few hundred meters are bound to be associated with errors in the details of $\mathbf{M}_{\mathbf{Th}}$. Our hope is that the gross qualitative picture presented here reflects that of the real ocean.

Below the top 1000 m, there is no clear sign of M advection or radiation by the model GS. The only exception may be wave radiation from a band that extends toward east-northeast from the southwest corner of the domain below 2000 m (Plate 3e). This band is located underneath the tongue of high $\bar{q}$ at 901 m, suggesting that waves radiating away from this area may represent an indirect influence of the GS at ~1000 m. At these deep levels the fluxes are predominantly westward and converge at the western boundary, where some M is dissipated by friction and some is advected by the boundary current. As noted earlier, the model substantially underestimates $\bar{\mathbf{V}}_{\mathbf{h}}M$ by the GS below the top few hundred meters, as well as the eddy kinetic energy. It implies that the import of wave activity along the model GS and subsequent wave radiation from the GS at these depths are also likely to be significantly underestimated. A comparison of the Deep Western Boundary Current (DWBC) in the model and the observed data [*Hogg*, 1983; *Hogg et al*., 1986; *Pickart and Smethie*, 1993] shows that the model also significantly underestimates the DWBC, particularly below 2000 m where the observed data show the strongest DWBC. Given the important role of the DWBC in the dynamics of the GS in the vicinity of the separation point found in idealized model experiments [e.g., *Thompson and Schmitz*, 1989;

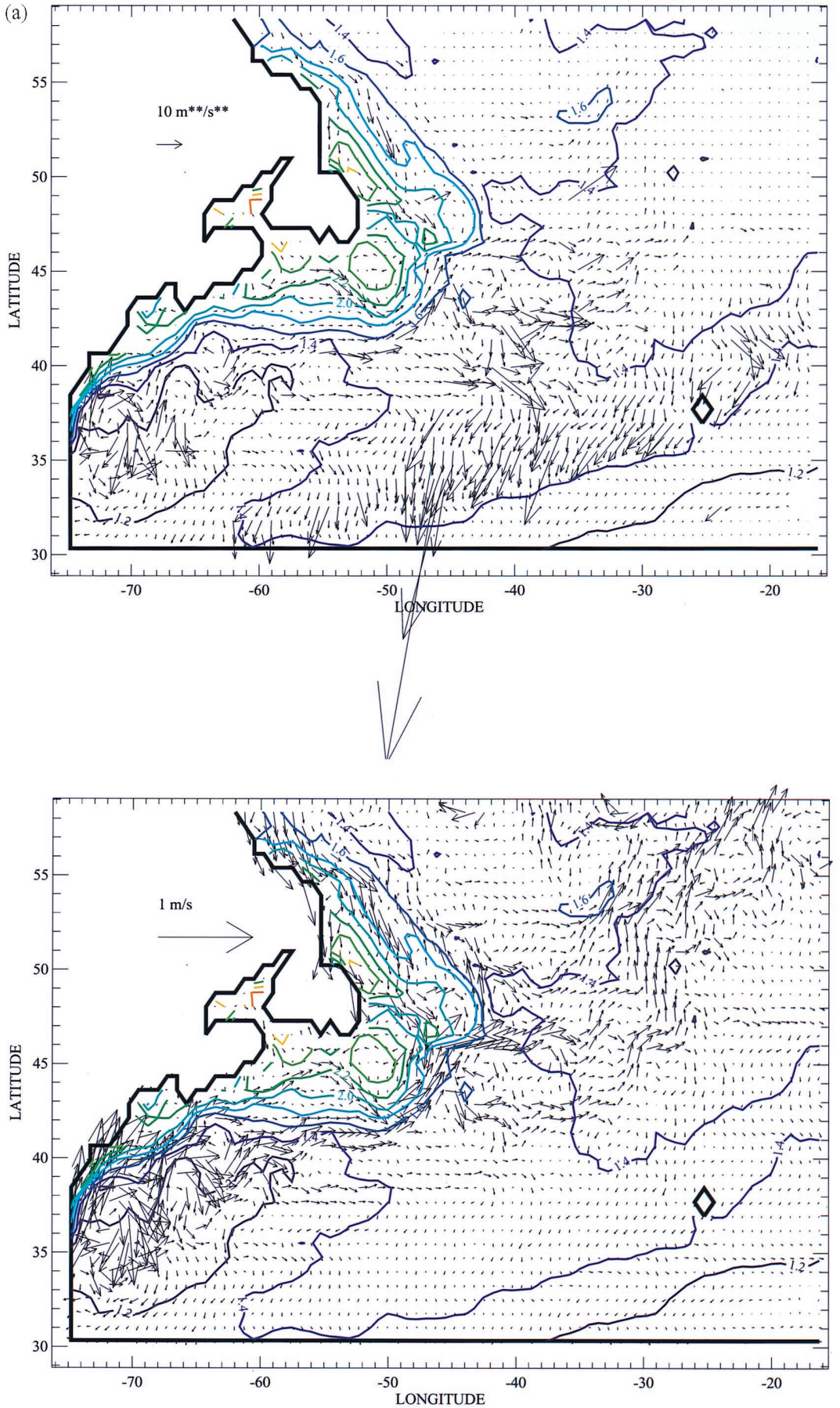

Plate 3. Vector plots of (top) $\mathbf{M_{Th}}$ and (bottom) $\bar{\mathbf{V}}_{\mathbf{h}}$ superimposed on contours of $\bar{q}$ at (a) 17, (b) 140, (c) 577, (d) 1375, (e) 2375, and (f) 3375 m. Units of $\bar{q}$ and $\mathbf{M_{Th}}$ are 1×10^{-4} s^{-1} and m^2 s^{-2}, respectively.

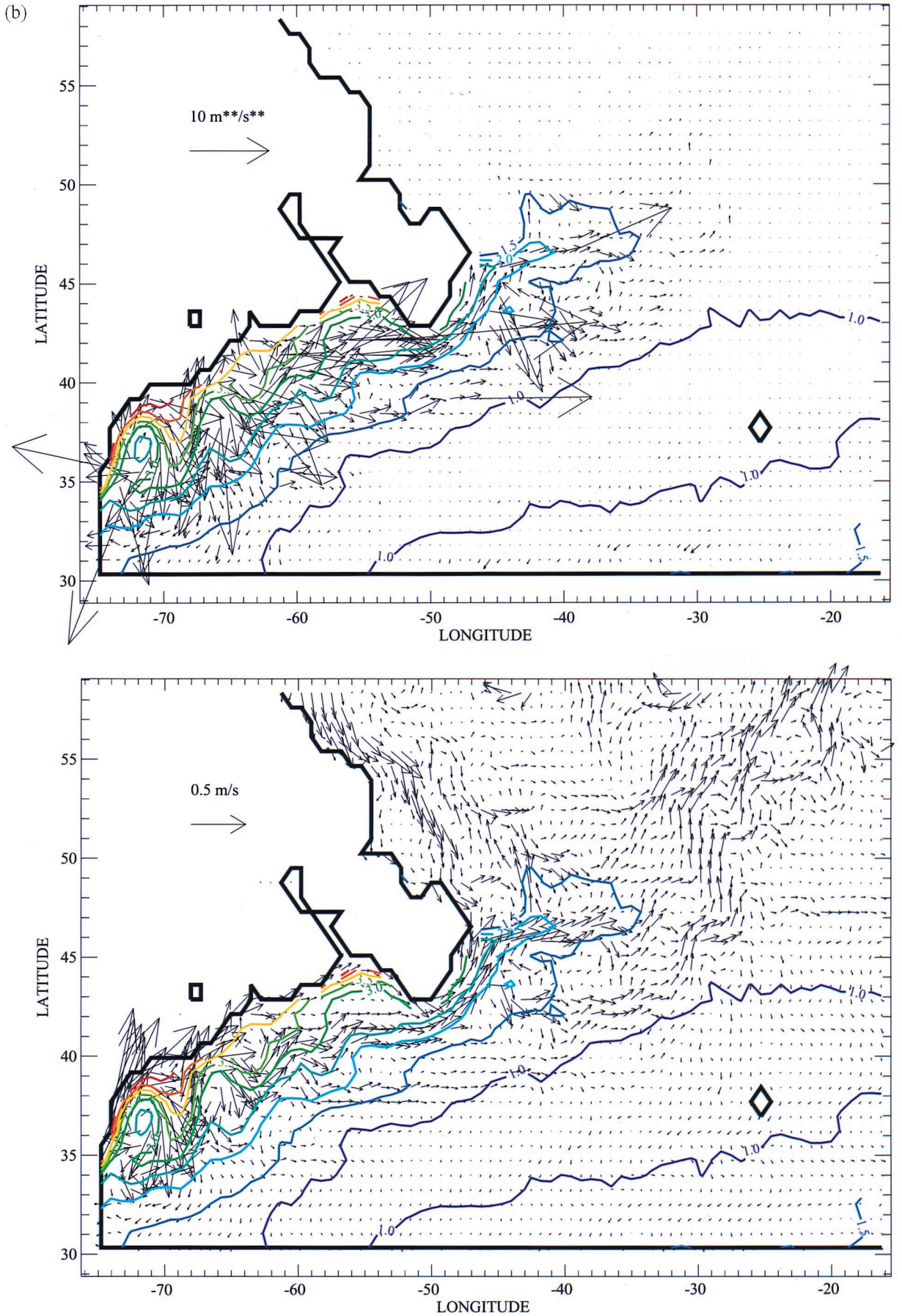

Plate 3. (continued)

(c)

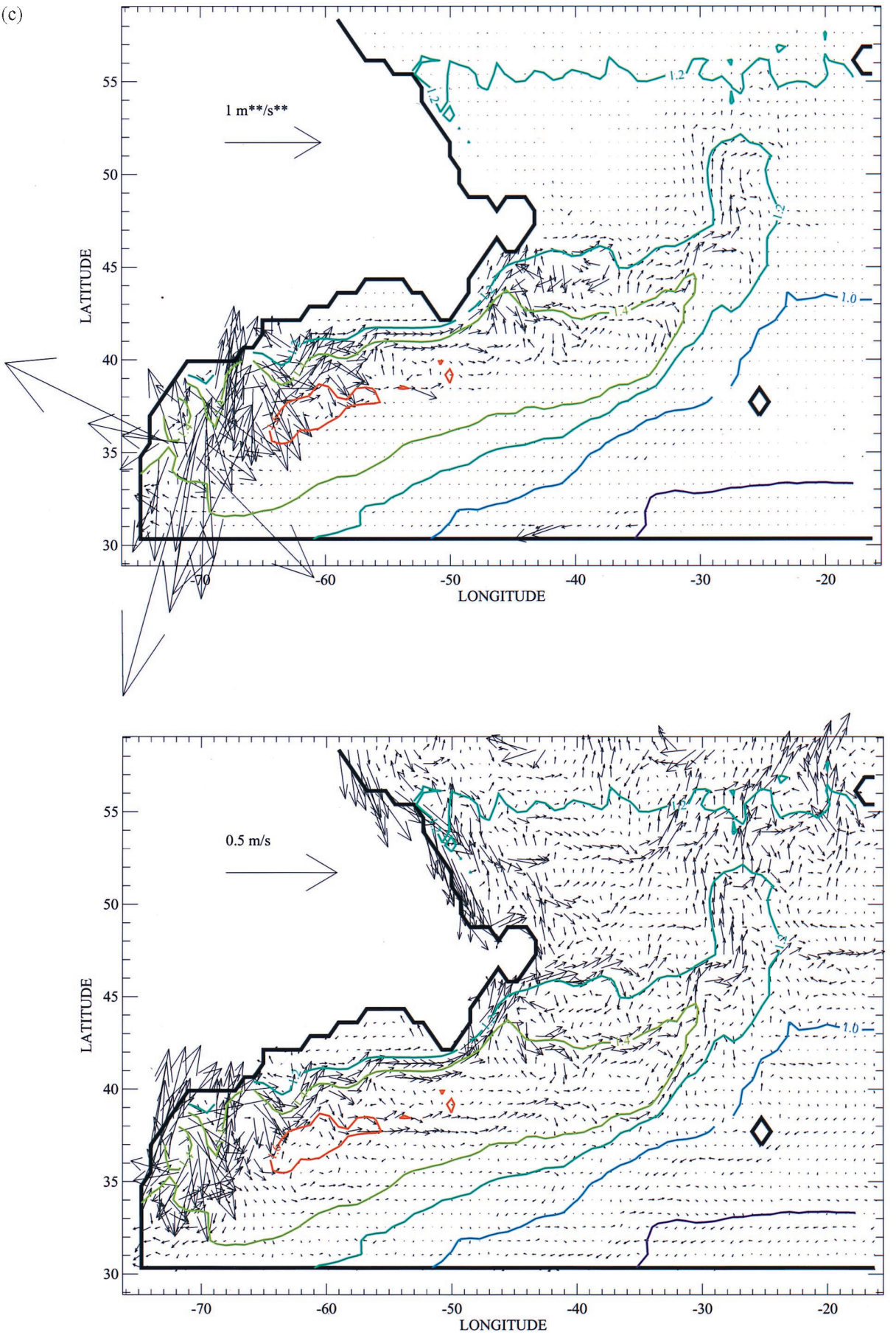

Plate 3. (continued)

(d)

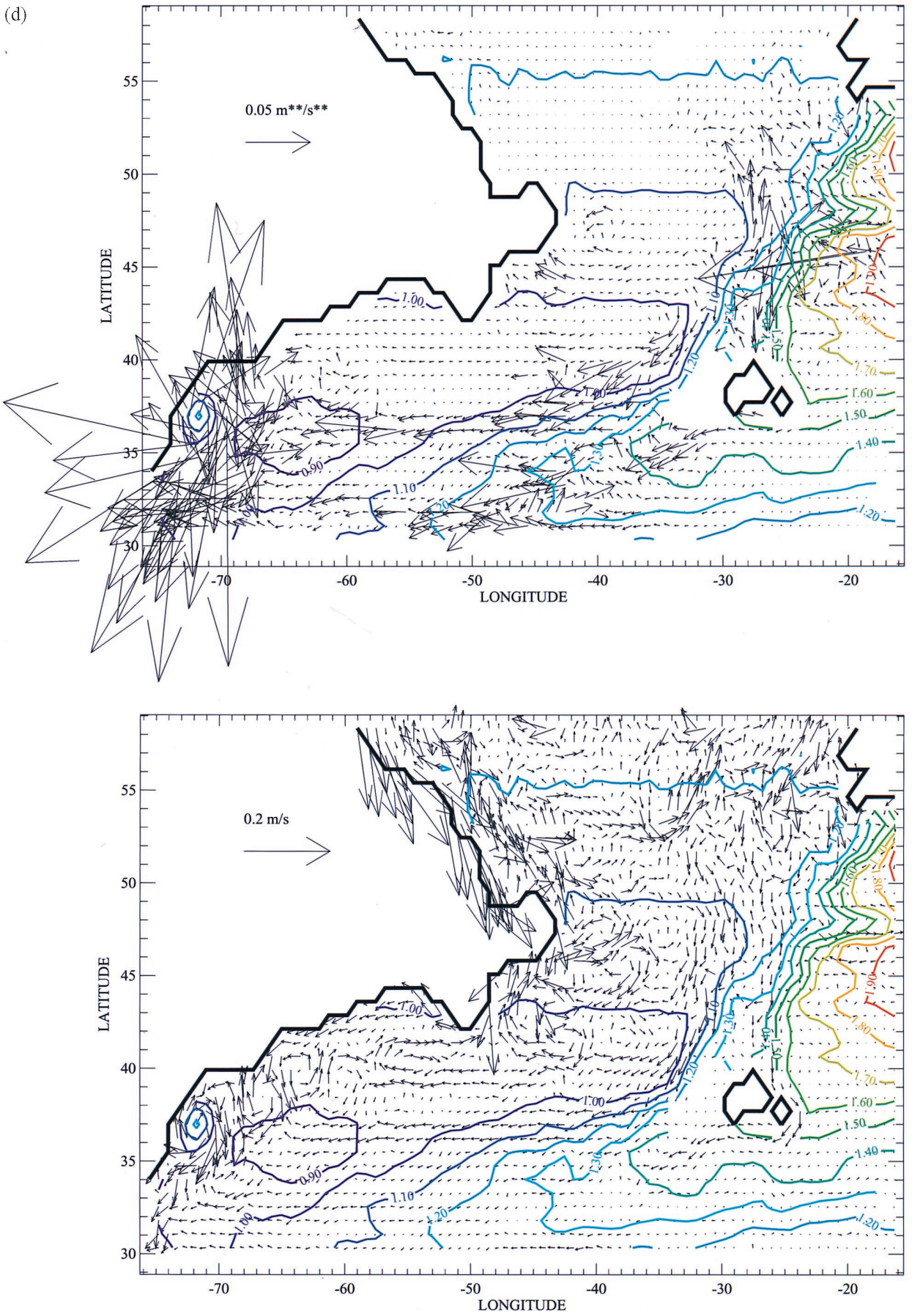

Plate 3. (continued)

(e)

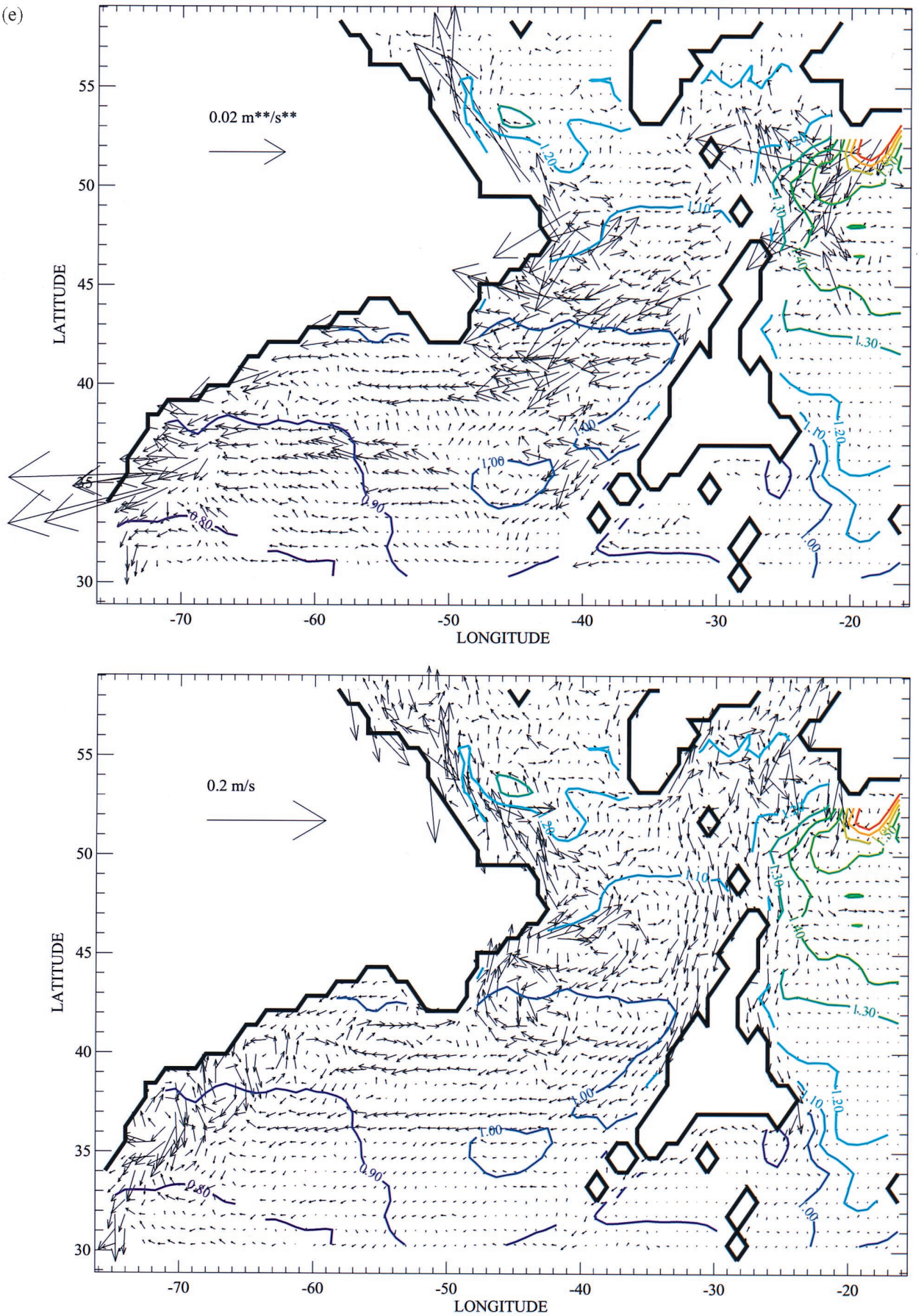

Plate 3. (continued)

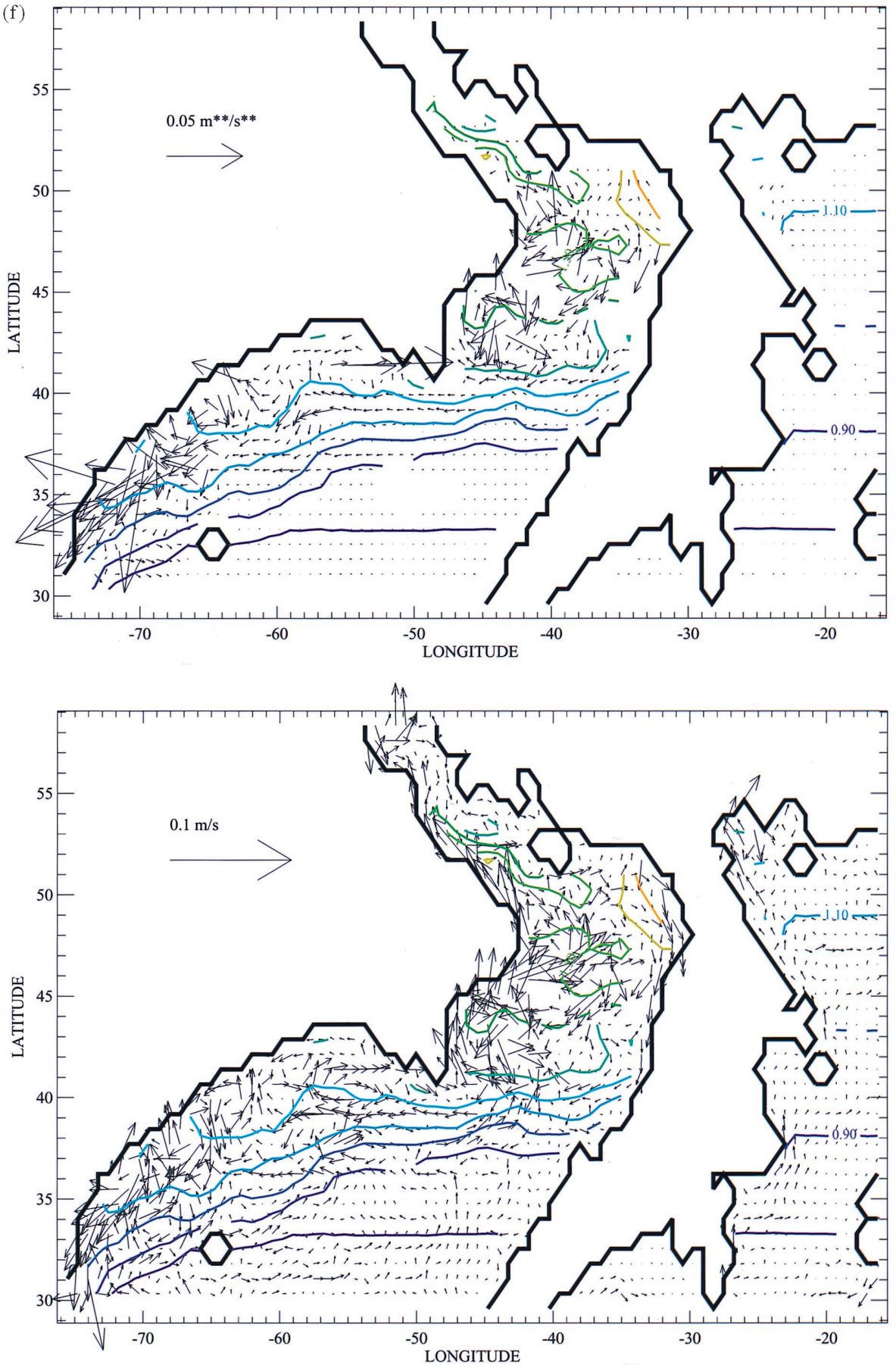

Plate 3. (continued)

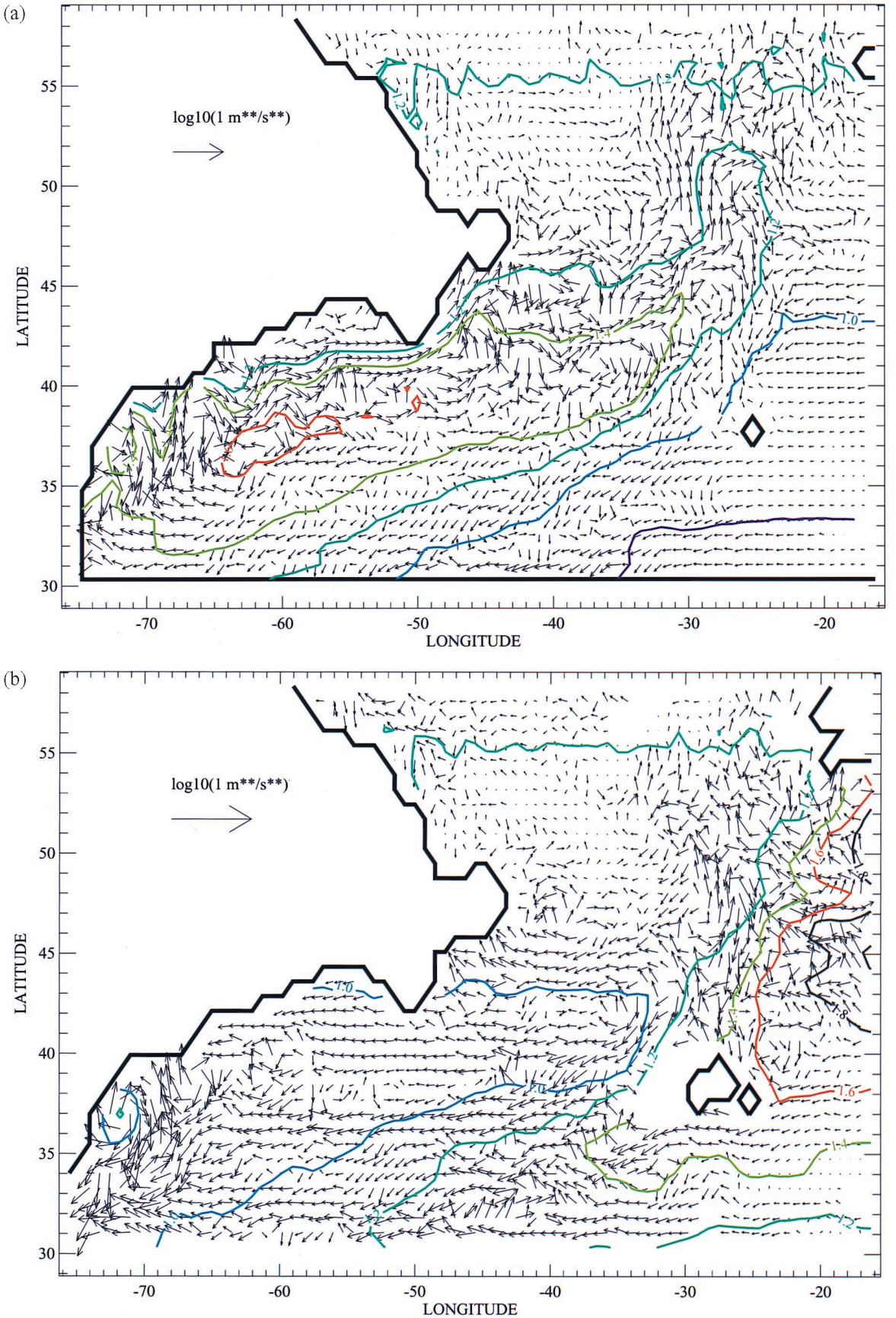

Plate 4. Vector plots of $\log_{10}(|\mathbf{M_{Th}}|)\mathbf{m}$, where $\mathbf{m}$ is a unit vector parallel to $\mathbf{M_{Th}}$, superimposed on contours of $\bar{q}$ at (a) 577 and (b) 1375 m. Before $\log_{10}(|\mathbf{M_{Th}}|)$ was calculated, $|\mathbf{M_{Th}}|$ was multiplied by 100 to make $\log_{10}(|\mathbf{M_{Th}}|)$ zero when $|\mathbf{M_{Th}}| = 0.01\ \mathrm{m^2\ s^{-2}}$. Negative values of $\log_{10}(|\mathbf{M_{Th}}|)$, i.e., $|\mathbf{M_{Th}}| < 0.01\ \mathrm{m^2\ s^{-2}}$, were set to zero.

Spall, 1996a, b], the underestimated DWBC in the model is likely to have resulted in errors in $\mathbf{M_{Th}}$ in the vicinity of the GS.

Chester et al. [1994] calculated wave activity fluxes to the south of the GS in a similar fashion and found that the horizontal component is generally southward at both 500 and 1000 m. The model shows the nonnegligible westward component at the 577 m level and the eastward component at the 1175 m level in the area considered by Chester et al., 55°W and 37°N. However, as is evident in Plate 4, the direction of $\mathbf{M_{Th}}$ varies significantly in space with a fairly small spatial scale. Since the model GS is far from perfect and the calculations by Chester et al. do have some uncertainty intrinsic to the data and error arising from the neglect of $\partial\bar{q}/\partial x$ and $\bar{\mathbf{V}}_\mathbf{h}M$, it is not surprising to see some difference in the direction of the fluxes in the model and their data. The important feature in agreement is the general pattern of wave radiation from the GS to its south both in data and in the model.

Another conspicuous feature in $\mathbf{M_{Th}}$ is the generation and radiation of wave activity in and around the Mediterranean Outflow. This feature is observed in the top 50 m and between 900 and 2500 m. Very large $\mathbf{M_{Th}}$ occurs in the band of large M over the edge of the Mediterranean Outflow in the top 50 m (Plate 3a). The large $\mathbf{M_{Th}}$ is almost entirely due to $\bar{\mathbf{V}}_\mathbf{h}M$ despite the weak mean flow in this region. The fluxes originate near the northern edge of the band and converge near the southern edge of the band, where the largest values in M are observed. Presumably, baroclinic waves begin to grow near the northern edge of the band and reach their maximum amplitudes and begin to decay near the southern edge as they are advected southward by the relatively weak mean flow in the region. Between 50 and 1000 m or so, there is no sign of significant wave radiation in this region. Between 1000 and 2500 m, $\mathbf{M_{Th}}$ shows propagation of waves, originating mostly in the southern half of the eastern boundary of the domain and eastern half of the southern boundary of the domain, primarily along the contours of $\bar{q}$ formed by the Mediterranean Outflow (Plate 3e). This is easier to see in a plot of $\log_{10}(|\mathbf{M_{Th}}|)\mathbf{m}$ (Plate 4b). The present diagnosis does not show from where the fluxes are originating. However, stability analysis and model experiments reported by *Spall* [1994] suggest that baroclinic instability may generate wave activity in the open ocean in and around the salt tongue of the Mediterranean Outflow, which may be the source of these wave activity fluxes. Near the edge of the high-$\bar{q}$ water generated by the Mediterranean Outflow we observe some westward and southwestward radiation and advection of wave activity. The source of these fluxes is presumably local baroclinic instability of the kind discussed by *Spall* [1994].

Below 2000 m the mean flow is fairly strong and flowing southward and southwestward along the western side of the MAR. Apparently, the strong flow over the topography generates some waves that radiate away from the MAR westward at these levels (Plates 3d and 3e), while it also advects substantial wave activity along the MAR. The westward $\mathbf{M_{Th}}$ emanating from the boundary appears to grow to some extent, suggesting that the waves excited by the topography grow or other sources of M, such as the indirect effect of the upper level GS, also generate waves off the boundary of the MAR. Most of the westward fluxes originating at the boundary appear to converge at the western boundary. Although the MAR does not provide a physical boundary above 2000 m, its indirect influence on wave propagation between 1000 and 2000 m is clear; wave activity fluxes originating to the east of the MAR are mostly contained to the east of the MAR. Trajectory calculations of particles show that horizontal particle movement between 1000 and 2000 m is also strongly influenced by the indirect effects of the MAR; particle trajectories show the presence of a very strong boundary against mixing above the MAR. Potential vorticity fields calculated from an improved hydrographic data set by *Lozier* [1997] suggest that the mixing barrier may exist in the real ocean also.

We examined convergence of $\mathbf{M_{Th}}$ for any clear relationship with the mean flow but have not identified a robust relationship, mainly because of the extreme noisiness of the convergence field. We also examined the propagation characteristics suggested by $\mathbf{M_{Th}}$ against movies of q field evolution and found that waves and packets of waves do appear to propagate in the manner suggested by $\mathbf{M_{Th}}$ fields. Thus, despite the limitation imposed by the simplifying assumptions used in deriving the formula, calculated $\mathbf{M_{Th}}$ shows the correct first-order propagation characteristics of transient waves in the vicinity of the model GS.

4.3. Vertical Fluxes

The vertical fluxes of transient wave activity in the model are expected to arise from motions associated with baroclinic waves for the most part. One may thus expect predominantly downward fluxes as the available potential energy provided by the surface forcing is released and converted into kinetic energy by baroclinic waves. *Chester et al*. [1994] found mostly downward fluxes in their calculations for a small area near 55°W and 37°N at 500 and 1000 m, in agreement with this expectation. Figure 1 shows M_{Rz} at selected levels. Near the surface, M_{Rz} is extremely noisy, and there are many small areas of upward fluxes, contrary to the expectation of primarily downward fluxes (Figure 1a). Unlike the horizontal component described above, M_{Rz} is negligible at all depths in the southeastern part of the domain, where the influence of the Mediterranean Overflow appears to generate fairly large horizontal wave activity fluxes. Large M_{Rz} for each depth is observed along the GS and underneath the GS at all depths. Below the top 300 m the area of downward fluxes is visibly larger than that at upper levels, but many isolated areas of upward fluxes still exist (Figure 1b). Below 1000 m, finally, M_{Rz} is primarily downward (Figure 1c). The decreasing noisiness in M_{Rz} with depth suggests that the extreme noisiness in the upper layers is not necessarily totally due to the relatively short averaging period used here. When M_{Rz} is averaged in the horizontal at each level, weighted by the area, it is downward at all levels, suggesting that energy released at upper levels through baroclinic instability propagates downward when the entire domain is considered.

There are two regions that show upward fluxes that are presumably caused by flows over topography. One is a narrow region along the western boundary near 73°W below 1875 m (Figure 1c). The upward flux is observed all the way to the bottom where the strong mean flow contacts the boundary, suggesting the possibility that the upward flux is a result of the flow over the topography. Another region is a narrow band on the western side of the MAR below 2375 m (Figure 1c). Although not as large as that seen near the separation point, there are upward fluxes along the western side of the MAR where substantial southward mean flow parallels the boundary. Note that flow modification in upper levels induced by these topography-generated upward wave activity fluxes may be, despite their small magnitudes, substantial because of the highly nonlinear nature of the flows at the upper levels.

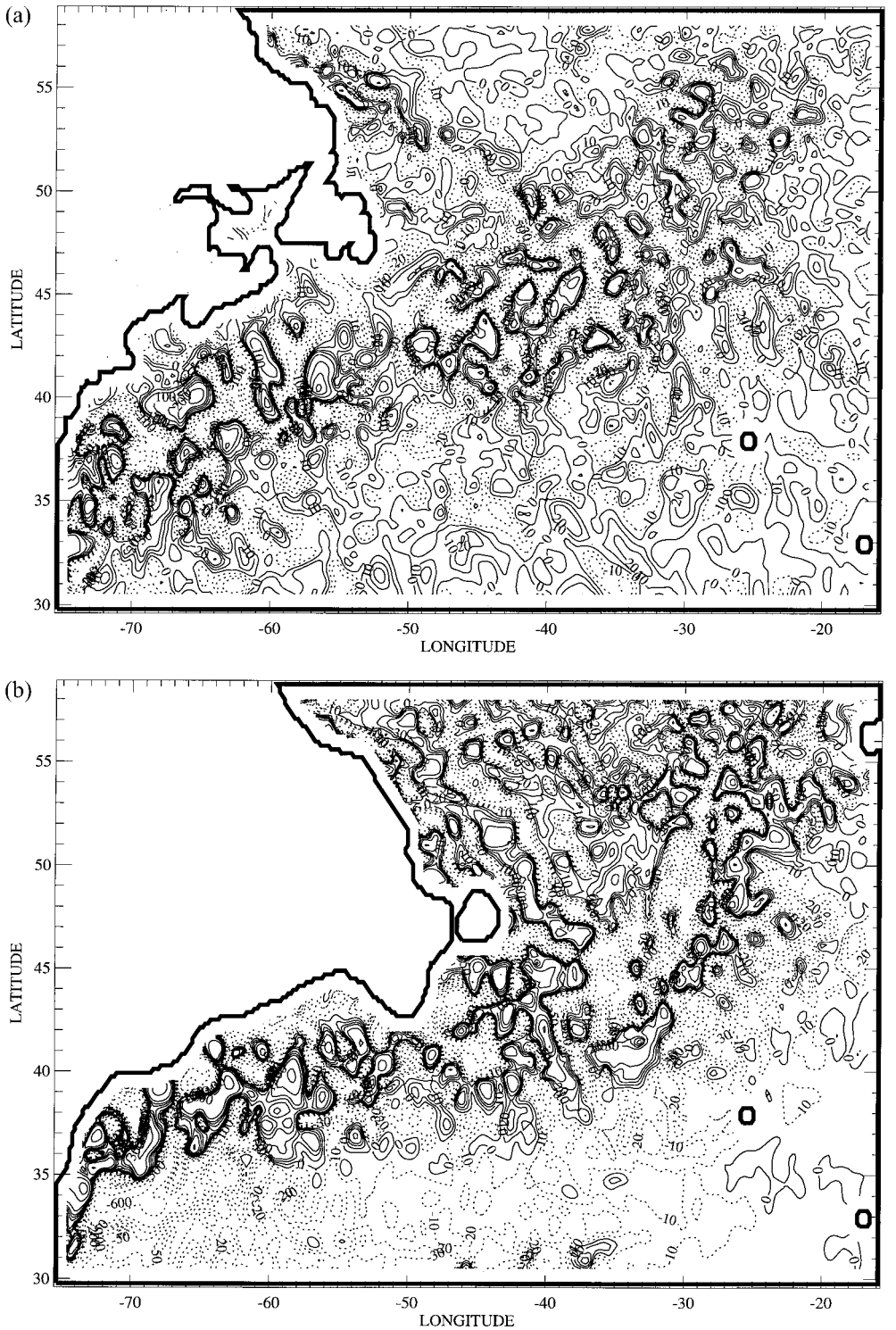

Figure 1. Contours of M_{Rz} at (a) 17, (b) 577, and (c) 2875 m. Units are 1×10^{-6} m^2 s^{-2}. Contour values shown are −1000, −600, −300, −200, −150, −100, −50, −30, −20, −10, 0, 10, 20, 30, 50, 100, 150, 200, 300, 600, and 1000 for Figures 1a and 1b and −600, −300, −200, −150, −100, −50, −30, −20, −10, 5, 0, 5, 10, 20, 30, 50, 100, 150, 200, 300, and 600 for Figure 1c. Negative values are dashed.

5. Eddy Forcing of Large-Amplitude Meanders in the Model GS

An interesting feature of the GS is quasi-stationary meanders that fluctuate slowly in time [e.g., *Halliwell and Mooers*, 1983; *Watts et al*., 1995]. We observe similar quasi-stationary meanders in the model solutions. As noted by *Chao et al*. [1996] and Nakamura and Chao (submitted manuscript, 2000b), however, the amplitudes of the large quasi-stationary meanders of the model GS just downstream of the separation point are considerably overestimated; while the observed quasi-stationary meanders have amplitudes of tens of kilometers

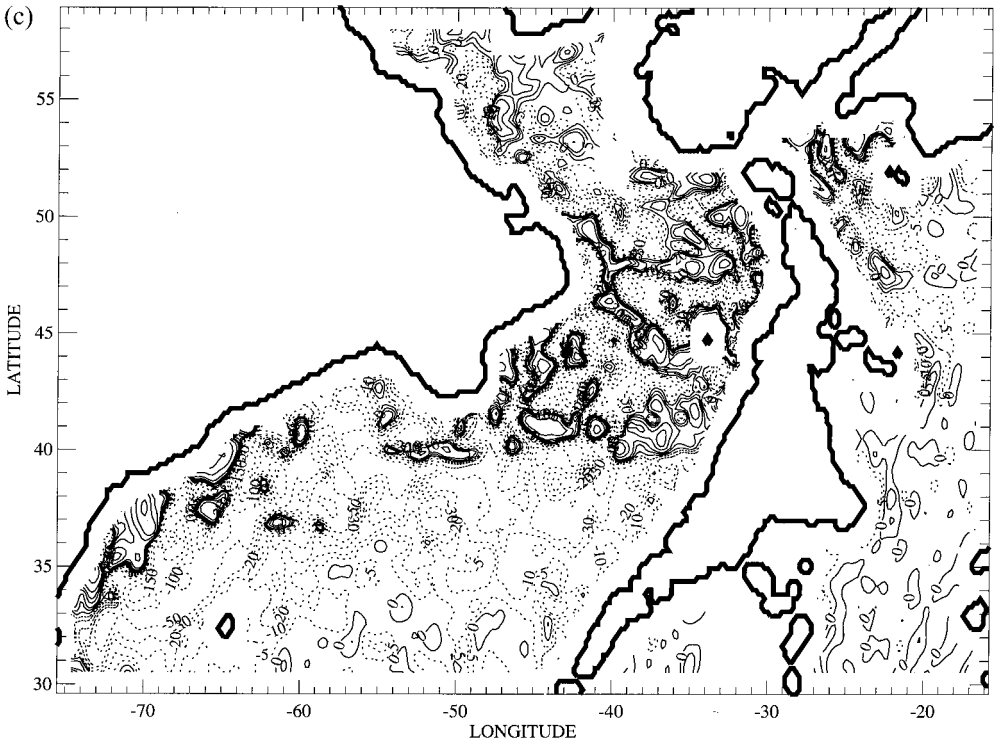

Figure 1. (continued)

[e.g., *Halliwell and Mooers*, 1983; *Watts et al*., 1995], the meanders in the model have amplitudes of a few hundred kilometers. Here we examine the relationship between the time mean flow and eddies and its role in the large-amplitude meanders in the model GS. Plate 5 shows the mean flow at 140 m, superimposed on $\bar{q}$, in the vicinity of the meanders downstream of the separation point. The overestimated amplitudes of the meanders are likely to be linked to other unrealistic features of the model. One likely consequence is a weakening of the flow farther downstream since the large meanders are sites of enhanced momentum dissipation in the model. It also results in underestimated heat and salt transport by the GS downstream of the separation point. The meanders are quasi-stationary, while their amplitudes fluctuate in time. Nakamura and Chao (submitted manuscript, 1999b) diagnosed the relationship between the mean and transient eddies at the meanders and concluded that the meanders are reinforced by the eddies. The relationship between the mean and eddies is very similar to that found in studies of atmospheric blocking events that are essentially large persistent meanders of the subtropical jet [e.g., *Shutts*, 1983; *Illari and Marshall*, 1983; *Nakamura*, 1998]. *Nakamura et al*. [1997] studied composite blocking events and found that wave activity fluxes converge in the region of the European blocking ridge in the amplification stage of the quasi-stationary wave that characterizes the blocking. They also found that wave activity fluxes radiate away from the blocking ridge as the blocking begins to dissipate. We find here a relationship between the wave activity fluxes and the ridges of the time mean meanders similar to that found by *Nakamura et al*. [1997] for their composite European blocking.

Plate 6 shows $\mathbf{M_{Th}}$ and $-\nabla_h \cdot \mathbf{M_{Th}}$, superimposed on $\bar{q}$, in the vicinity of the meanders at 140 m level. There is a small area of strong $\mathbf{M_{Th}}$ convergence (positive values of $-\nabla_h \cdot \mathbf{M_{Th}}$) along the upstream rim of the ridge at the first meander after the separation point. The area is a relatively small portion of the entire ridge at the first meander. At the second meander, downstream of the first meander, there is a clear sign of $\mathbf{M_{Th}}$ convergence in a substantial portion of the upstream half of the ridge. This pattern indicates that horizontal wave activity fluxes converge in the meandering ridges, tending to amplify the ridges. It also implies that transient wave activity is dissipated there. The weaker sign of meander amplification by transient eddies at the first meander suggests that stationary wave forcing, such as topographic forcing, may be more important in forcing the first meander. Similar patterns of $\mathbf{M_{Th}}$ convergence in the ridges are observed at other levels in the top 1000 m of the model. This relationship between the meanders and $\mathbf{M_{Th}}$ is in agreement with the conclusion drawn by Nakamura and Chao (submitted manuscript, 1999b); transient eddies tend to reinforce the meanders. As reported by *Nakamura et al*. [1997], the weak flow inside the ridges provides a favorable condition for accumulation of wave activity, which in turn results in further amplification of the ridges. Note that this suggests a positive feedback between the mean flow and eddies at the meanders.

The relationship between transient eddies and the time mean meanders found here suggests that amplitude fluctuations of the quasi-stationary meanders in the GS may be due to accumulation and discharge of wave activity in the region of meanders in a way similar to that which occurs in atmospheric blocking events reported by *Nakamura et al*. [1997]. It also suggests that the overestimated amplitudes of the quasi-stationary meanders in the model GS may be caused by a factor that results in an overestimated tendency for wave activity to converge in the meanders. On the basis of the diagnostic calculations of eddy enstrophy, eddy potential energy, kinetic energy, and eddy momentum fluxes we speculate that insufficient model resolution for baroclinic waves of deformation radius scales may result in underestimated zonal acceleration of the GS after its separation from the boundary, result-

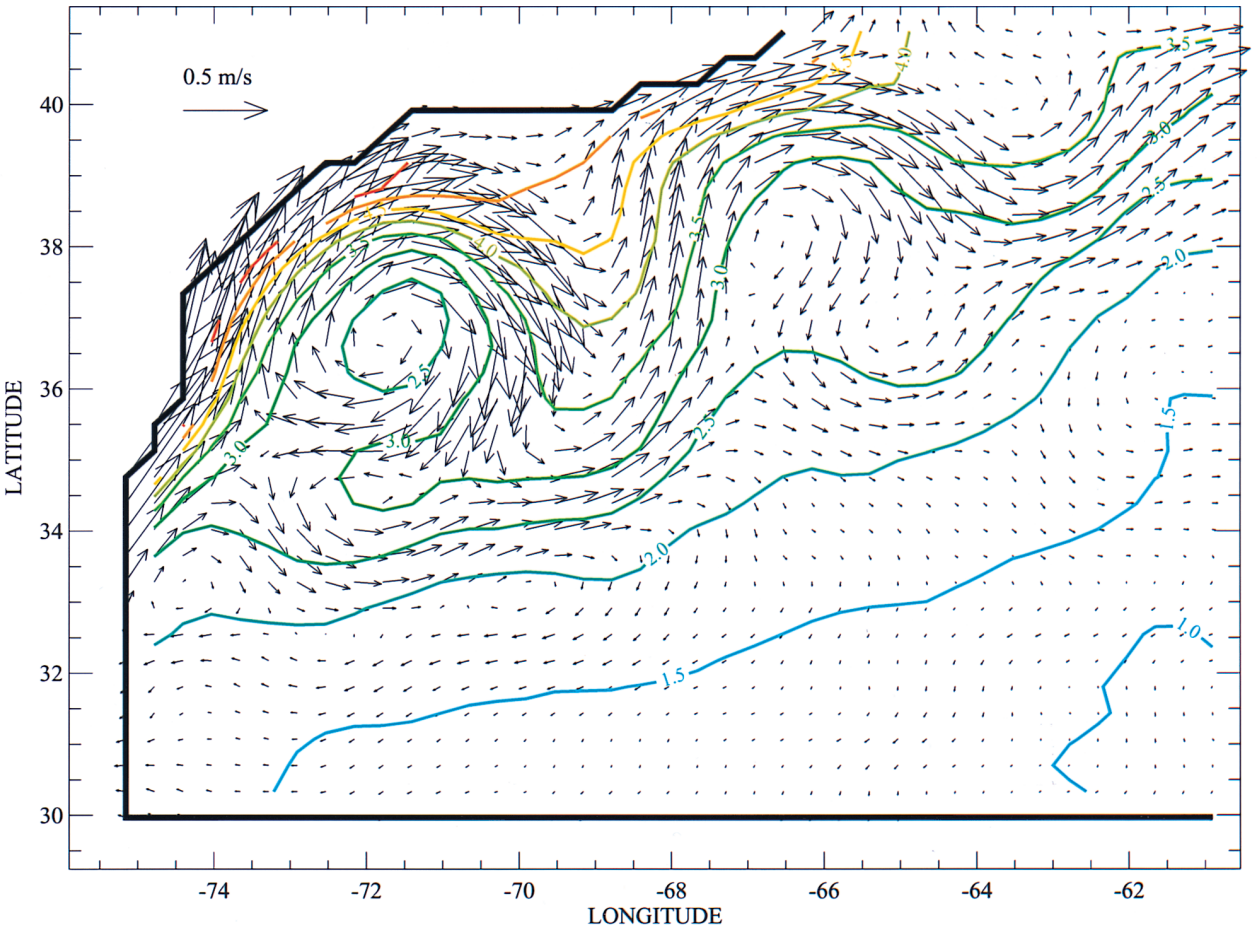

Plate 5. Vector plots of $\bar{\mathbf{V}}_\mathbf{h}$ superimposed on contours of $\bar{q}$ at 140 m. Units of the mean flow and $\bar{q}$ are m s^{-1} and 1×10^{-4} s^{-1}, respectively. Only the vicinity of the large meanders is shown.

ing in excessive accumulation of wave activity in the region of meanders. The underestimated zonal acceleration of the GS downstream of the separation point may create an unrealistic imbalance between the downstream advection of wave activity and input of wave activity immediately downstream of the separation point and trigger growth of the quasi-stationary meanders through the positive feedback action of eddies. Once the meanders are created, eddies will keep reinforcing the meanders, in which dissipation of eddy potential enstrophy is enhanced to compensate for the underestimated downstream advection of eddy potential enstrophy and wave activity by the model GS. The sensitivity of the model kinetic energy along the GS to the model resolution reported by *Schmitz and Thompson* [1993] supports this scenario. Another possible cause of the unrealistically large meander amplitudes is an overestimated topographic forcing of stationary waves, reinforced by the positive feedback of transient eddies. Localized vertically coherent upward wave activity fluxes near the boundary in this region, mentioned earlier, support this possibility as well. Since the wave activity dissipation in the quasi-stationary meanders is also likely to be overestimated in the model, the overestimated amplitudes of the meanders are likely to have resulted in unrealistic features in the wave propagation characteristics, such as underestimated wave activity advection by the GS and underestimated wave radiation from the GS in the vicinity of and downstream of the quasi-stationary meanders.

6. Eddy Characteristics at 55°W

It is of some interest to examine characteristics of the eddy fields with respect to the zonal mean flow for possible systematic relationships between the mean flow and eddies at longitudes where observational data have been collected and examined. We have examined the vertical cross sections of the time mean zonal flow and eddy fields at 55°W since the peak of a weak recirculation to the north of the model GS is observed around this longitude. The time mean zonal flow is practically the same as the mean along-stream flow for the model GS at this longitude. Figure 2 shows vertical cross sections of $\bar{u}$, $\overline{u'v'}$, $-d/dy\ (\overline{u'v'})$, and M_T^y at 55°W. The model GS has an unrealistic secondary southern branch centered at 38°W (Figure 2a). The secondary branch is only half as strong as the main northern branch, which is situated ~2° north of the observed GS. Also, there is another even weaker third branch just off the coast to the north of the main branch. The splitting of the GS into three branches appears to be closely connected to the overestimated large-amplitude quasi-stationary meanders just downstream of the separation point. The main branch is significantly weaker than the observed GS at this longitude, in part, because of the splitting into three branches upstream. (Compare this, for example, with the zonal velocity cross section at 55°W shown by *Hall and Fofonoff* [1993].) Even with the main and the secondary branches combined, the model GS

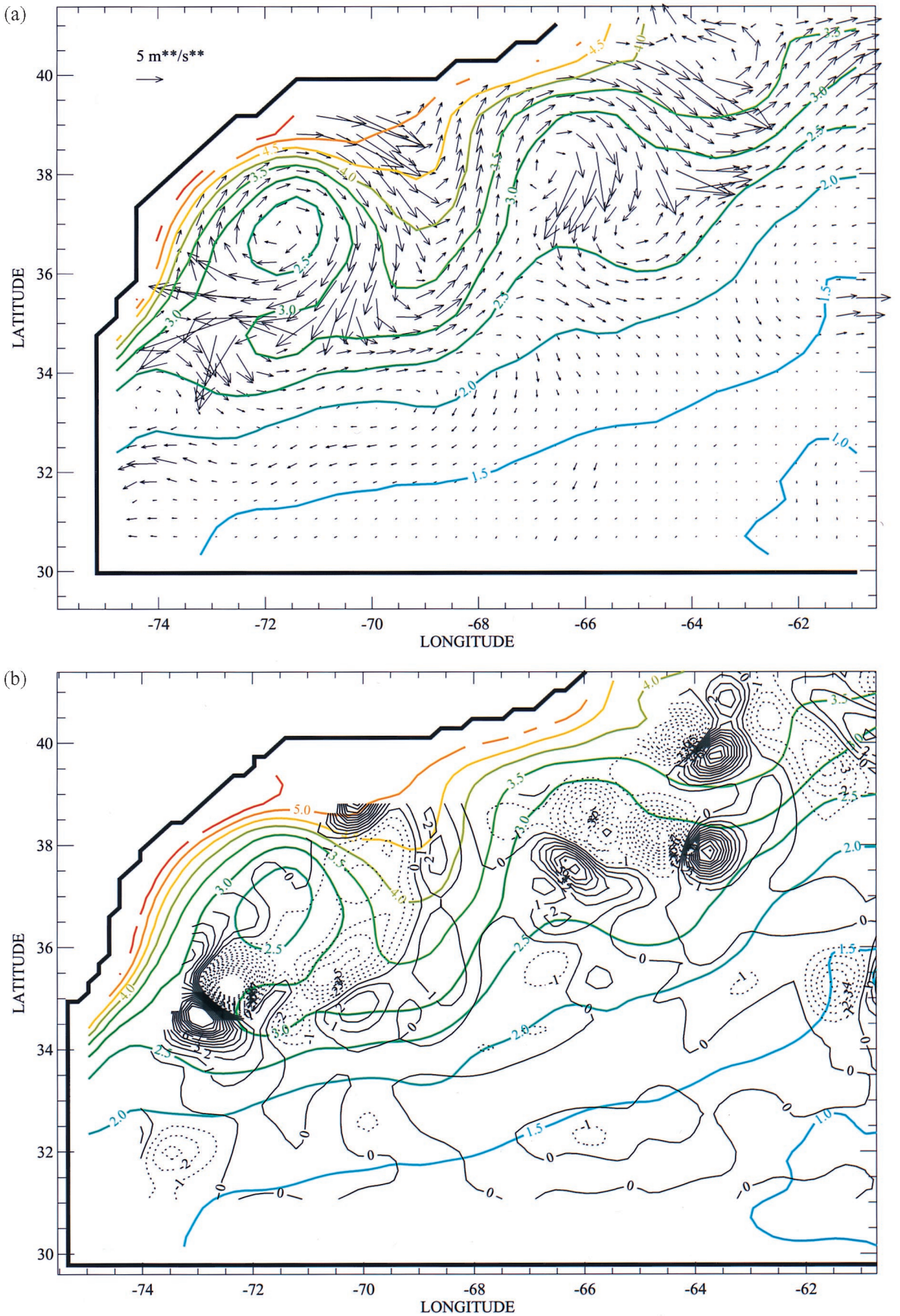

Plate 6. Vector plots of (a) $\mathbf{M_{Th}}$ and (b) $-\nabla_h \cdot \mathbf{M_{Th}}$ superimposed on contours of $\bar{q}$ at 577 m. Only the vicinity of the large meanders is shown. Units of $\mathbf{M_{Th}}$ and $\bar{q}$ are the same as in Plate 3. Units of $-\nabla_h \cdot \mathbf{M_{Th}}$ are $m^2\ s^{-2}\ d^{-1}$. The contour interval of $-\nabla_h \cdot \mathbf{M_{Th}}$ is 1 $m^2\ s^{-2}\ d^{-1}$.

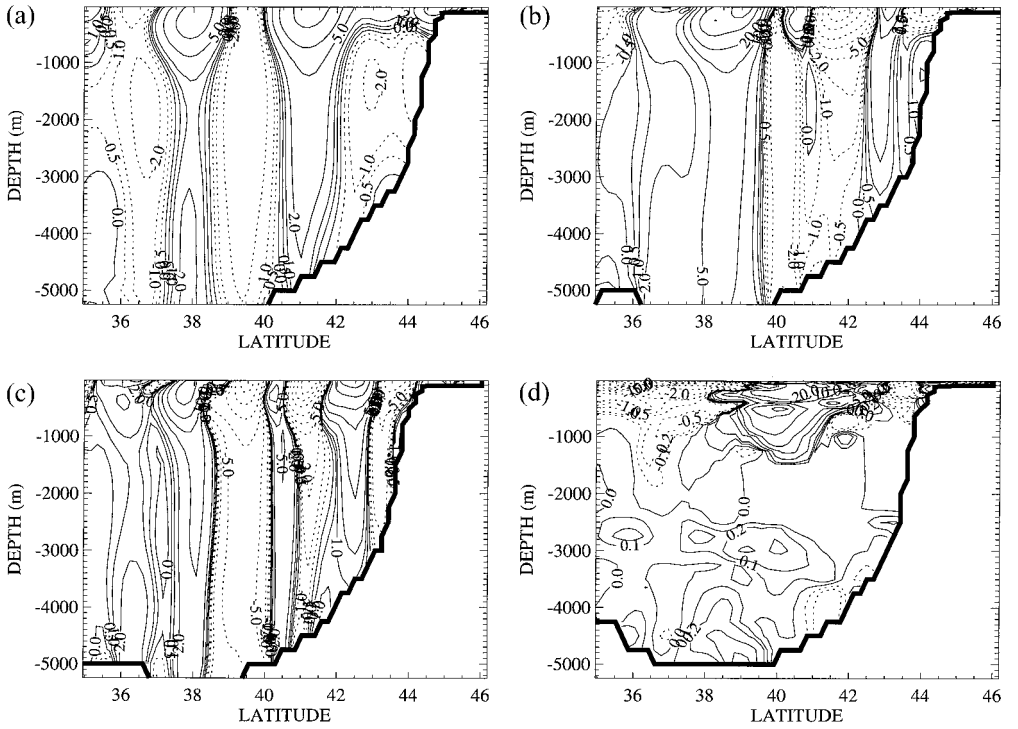

Figure 2. Cross sections of (a) $\bar{u}$, (b) $\overline{u'v'}$, (c) $-d/dy\ (\overline{u'v'})$, and (d) M_T^y at 55°W. Units are 10^{-2} m s^{-1}, 10^{-4} m^2 s^{-2}, 10^{-4} m s^{-1} d^{-1}, and 10^{-2} m^2 s^{-2}, respectively. Contour values shown are −100, −80, −60, −40, −20, −10, −5, −2, −1, −0.5, 0, 0.5, 1, 2, 5, 10, 20, 40, 60, 80, and 100 for Figures 2a–2d.

below the top few hundred meters is visibly weaker than the observed. Associated with the underestimated GS is the underestimated eddy kinetic energy, particularly below the top few hundred meters, as mentioned earlier. The model also generates recirculations to the north and south of the GS in a qualitative agreement with the observation. However, again, the recirculations are displaced, and strengths of the recirculations are weaker than the observed [e.g., cf. *Hogg et al*., 1986; *Hall and Fofonoff*, 1993]. Presumably, these discrepancies between the model recirculations and the observed recirculations are closely connected to the unrealistic features of the model GS, such as the northward displacement in the position of the GS, splitting of the GS, and the underestimated strength of the GS. Despite these problems in the model-generated GS and recirculations it seems useful to examine the eddy fields with respect to the recirculations to potentially learn the qualitative relationship between the recirculations and eddies.

The meridional wave radiation shown in the cross section of M_T^y suggests wave radiation from the model GS in the upper 500 m or so as described in section 4 (Figure 2d). (There are only minor differences between the cross sections of M_T^y and M_R^y.) However, a close inspection of the cross sections reveals that the core of the wave radiation is located in between the main and the southern branches of the model GS. Interestingly, the radiation core is located very close to the observed GS. In the immediate vicinity of the northern boundary the wave radiation is away from the boundary from the top to the bottom with a very small exception at ~2500 m. In most of the interior below 1000 m, wave radiation is very weak and predominantly northward. These patterns of wave radiation suggest that waves radiated from the model GS and from the northern boundary are converging off the northern boundary at all depths, perhaps contributing to the northern recirculation in the model. *Bower and Hogg* [1992] found evidence of barotropic wave radiation from the deep GS and found $\overline{u'v'}$ to be positive and negative to the south and north of the GS, respectively. In the model this is reproduced to some extent. In the top 700 m the boundary between positive and negative $\overline{u'v'}$ coincides well with the core of the main branch of the GS (Figure 2b). However, the boundary is at ~40°N in the band of weak westward flow between the main and the secondary branch of the model GS below the top 700 m. This may well be related to the unrealistic features in the model GS and underestimated kinetic energy below the top few hundred meters in the model. The cross section of $-d/dy\ (\overline{u'v'})$ shows acceleration of $\bar{u}$ due to the convergence of $\overline{u'v'}$ (Figure 2c). A careful inspection of Figure 2c shows that $\overline{u'v'}$ tends to accelerate $\bar{u}$ in the westward core of both the southern and northern recirculations and also the core of the main branch of the GS. On the other hand, it clearly tends to decelerate $\bar{u}$ in the core of the unrealistic southern secondary branch of the GS and the narrow band of westward flow between the main and the secondary branches. *Hogg* [1983] suggested that the northern recirculation may be forced by interfacial form drag induced by eddies. The present results support his hypothesis despite some obvious model difficiencies in reproducing observed features and despite some obvious model difficiencies in accurately reproducing the observed circulations.

7. Summary and Discussion

We have used the three-dimensional quasi-geostrophic transient wave activity flux diagnostic developed by *Plumb* [1986] to examine characteristics of transient eddy generation, propagation, and dissipation (or absorption) in the vicinity of the GS in an eddy-resolving model of the North Atlantic. The results show evidence of wave radiation from the model GS, particularly clearly to the south of the GS, in agreement with limited

calculations using observed data by *Bower and Hogg* [1992] and *Chester et al*. [1994]. The gross pattern of wave activity fluxes in the western North Atlantic is strong advection of wave activity by the GS and radiation of wave activity from the GS in the top 1000 m or so, suggesting a substantial source of wave activity in the vicinity of or farther upstream of the separation point. Horizontal wave activity fluxes tend to reinforce large-amplitude time mean meanders in the model GS just downstream of the separation point, in a way very similar to that observed in atmospheric blocking events. Below the top 1000 m, waves radiate primarily westward, originating from the lateral boundary or areas of vigorous baroclinic waves. Significant convergence of wave activity flux is observed at the western boundary at all depths. There are some signs of northward wave radiation from the GS and subsequent convergence in the vicinity of the westward flow of the northern recirculation. Eddy meridional flux of zonal momentum tends to force the westward flow of both the northern and southern recirculations in the model. Open ocean instabilities appear to generate large wave activity near the surface above the edge of the Mediterranean Outflow. The fluxes of wave activity originating from there are very large near the surface but are confined in a narrow band, presumably because of weak mean flow advection. The same open ocean instabilities appear to be responsible for generating relatively large wave activity and its fluxes in and around the Mediterranean Outflow between 1000 and 2500 m. Although the assumptions required for the derivation of the formula are not necessarily satisfied well in oceanic applications, visual inspections of movies of potential vorticity fields suggest that the diagnostic is capable of identifying the first-order horizontal propagation characteristics of quasi-geostrophic transient eddies in the model. The vertical flux of wave activity is extremely noisy in the top 1000 m, showing many small areas of both upward and downward fluxes. Below the top 1000 m it is mostly downward. When it is averaged horizontally at each depth, however, the vertical flux is downward at all depths, suggesting a conversion of potential energy supplied near the surface into kinetic energy by baroclinic waves.

Because of the expected long evolution timescales of the oceanic flows at various depths, one must note that the results presented here suffer from somewhat noisy mean fields and quite noisy eddy fields that arise from the relatively short period considered here. The annual mean flow of the 5 years considered here shows some sign of low-frequency variability at all depths. Also, deep levels of the model are almost certainly not in equilibrium after 30 years of integration. To assess the sensitivity of the present results to the time period considered, we repeated calculations of both the horizontal flux and the vertical flux for selected levels, using only the first 3 years of the 5 year output. We find that the overall features remain the same at all depths, both qualitatively and quantitatively. However, close inspections reveal some differences in the detail. In order to obtain smooth mean fields and wave activity flux fields, a much longer time series is probably necessary. The present results may be more appropriately interpreted as diagnoses of the relationship between low-frequency and high-frequency fields, where the low-frequency component is defined as that part of the time series that evolves with timescales longer than 5 years and the high-frequency component being the rest. We believe, however, that the gross features shown here would be present in diagnoses of a much longer time series also.

To what extent the current results represent the reality is not clear because of the lack of calculations of these diagnostic quantities with observed data with extensive spatial and temporal coverages. We also emphasize that unrealistic features in the model solution are associated with unrealistic features in the transient eddy propagation characteristics presented here. Of particular concern is the impact of the northward displaced and underestimated GS on the results presented here. In the top few hundred meters, where the model GS is reasonably strong, the picture presented here may be qualitatively correct. However, below the top few hundred meters, especially at the intermediate and deep levels where the model GS is extremely weak and unorganized, the picture presented here may be incorrect even qualitatively. For example, the deep GS may, in reality, advect a significant amount of wave activity from the separation point and radiate it along its path. Needless to say, the magnitude of transient wave activity fluxes is highly likely to be underestimated in the model at deep levels, because of the underestimated eddy energy. Also, the deduced unrealistically strong dissipation of the wave activity in the large-amplitude quasi-stationary meanders just downstream of the separation point is likely to have resulted in underestimated wave radiation from the GS downstream of the meanders. These unrealistic features are likely to have affected the entire GS system, including the DWBC and recirculations. One must be aware of these limitations that arise from model difficiencies in a diagnosis of this kind. We believe that some aspects of transient wave propagation characteristics will be improved in a higher-resolution model but not necessarily all aspects. For example, we expect eddy fields at high latitudes, in general, to be represented better by higher resolution because of the smaller radii of deformation at higher latitudes. We also suspect that the component of $\mathbf{M}_{\mathbf{Th}}$ that is perpendicular to contours of $\bar{q}$ would be larger in a higher-resolution model output because of the greater eddy kinetic energy generated by the higher resolution. Regions whose eddy fields are dominated by local processes (e.g., in and around the water influenced by the Mediterranean Outflow) are, in general, likely to benefit from a higher resolution. On the other hand, regions whose eddy fields are significantly affected by nonlocal processes (e.g., the vicinity of the GS) do not necessarily receive the benefits of a higher resolution. Various factors other than the model resolution are known to have significant impact on model performance on simulating the separation and path of the GS [e.g., *Thompson and Schmitz*, 1989; *Dengg*, 1993]. Thus an improvement in eddy fields in the vicinity of the GS is not guaranteed by a higher-resolution model.

Given very important roles of transient eddies in the maintenance of and fluctuations in the ocean circulations and climate, characteristics of wave generation, propagation, and dissipation need to be studied in detail. We have here demonstrated that the diagnostic of the three-dimensional transient wave activity fluxes developed by *Plumb* [1986] may be a powerful diagnostic tool for oceanic problems. We found the physical nature of the information provided by the diagnostic to be insightful in examining the model output. It may not be very useful in quantifying the impact of eddies on the mean or low-frequency state, but it seems to be useful in learning the qualitative relationship between the eddies and the mean or low-frequency state. It may thus also help us deduce the physical processes involved in generating a certain type of unrealistic feature, i.e., those features that involve eddy forcing, in model solutions when applied to model output. Once the wave activity fluxes are calculated from observational data with a reasonable accuracy in the future, the fluxes computed from model output may be compared against the observed fluxes for a quantitative assessment of the difficiencies

in the model physics. Measuring quantities that are necessary to compute the wave activity and its fluxes in the vicinity of the GS will be of great scientific value not only in terms of learning the reality but also in terms of improving eddy-resolving models. We believe that the approach presented here will supply valuable information in such studies.

Acknowledgments. The research described in this paper was carried out by the Jet Propulsion Laboratory (JPL), California Institute of Technology, under contract with National Aeronautics and Space Administration. Computations were carried out on the 256-processor Cray T3D through the JPL Supercomputing Project. Nakamura is indebted to John Marshall for stimulating conversations that led to this series of diagnoses. Mike Spall kindly read the draft of this paper and gave us helpful comments. Finally, we wish to thank Paola Rizzoli and an anonymous reviewer for their comments, which helped improve the manuscript.

References

Beckman, A., C. W. Böning, C. Köberle, and J. Willebrand, Effects of increased horizontal resolution in a simulation of the North Atlantic Ocean, *J. Phys. Oceanogr*., *24*, 326–344, 1994.

Bower, A. S., and N. G. Hogg, Evidence for barotropic wave radiation from the Gulf Stream, *J. Phys. Oceanogr*., *22*, 42–61, 1992.

Bryan, F. O., and W. R. Holland, A high resolution simulation of the wind- and thermohaline-driven circulation in the North Atlantic Ocean, in *'Aha Huliko'a Parameterization of Small-Scale Processes*, edited by P. Muller and D. Henderson, pp. 99–115, Hawaii Inst. of Geophys., Honolulu, 1989.

Bryan, K., A numerical method for the study of the circulation of the world ocean, *J. Comput. Phys*., *4*, 347–376, 1969.

Chao, Y., A. Gangopadhyay, F. O. Bryan, and W. R. Holland, Modeling the Gulf Stream: How far from reality?, *Geophys. Res. Lett*., *23*, 3155–3158, 1996.

Chester, D. B., P. Malanotte-Rizzoli, J. Lynch, and C. L. Wunsch, The eddy radiation field of the Gulf Stream as measured by ocean acoustic tomography, *Geophys. Res. Lett*., *21*, 181–184, 1994.

Cox, M. D., A primitive equation, 3-dimensional model of the ocean, *GFDL Ocean Group Tech. Rep. 1*, Geophys. Fluid Dyn. Lab., Princeton, N. J., 1984.

Dengg, J., The problem of Gulf Stream separation: A barotropic approach, *J. Phys. Oceanogr*., *23*, 2182–2200, 1993.

Dukowicz, J. K., and R. D. Smith, Implicit free-surface method for the Bryan-Cox-Semtner ocean model, *J. Geophys. Res*., *99*, 7991–8014, 1994.

Eliassen, A., and E. Palm, On the transfer of energy in stationary mountain waves, *Geofys. Publ*., *22*, 1–23, 1961.

Hall, M. M., and N. P. Fofonoff, Downstream development of the Gulf Stream from 68° to 55°W, *J. Phys. Oceanogr*., *23*, 225–249, 1993.

Halliwell, G. R., Jr., and C. N. K. Mooers, Meanders of the Gulf Stream from Cape Hatteras 1975–1978, *J. Phys. Oceanogr*., *13*, 1275–1292, 1983.

Hogg, N. G., A note on the deep circulation of the western North Atlantic: Its nature and causes, *Deep Sea Res*., *Part A*, *30*, 945–961, 1983.

Hogg, N. G., Stochastic wave radiation by the Gulf Stream, *J. Phys. Oceanogr*., *18*, 1687–1701, 1988.

Hogg, N. G., R. S. Pickart, R. M. Hendry, and W. J. Smethie Jr., The northern recirculation gyre of the Gulf Stream, *Deep Sea Res*., *Part A*, *33*, 1139–1165, 1986.

Holland, W. R., The role of mesoscale eddies in the general circulation of the ocean: Numerical experiments using a wind-driven quasi-geostrophic model, *J. Phys. Oceanogr*., *8*, 363–392, 1978.

Holland, W. R., and P. B. Rhines, An example of eddy-induced ocean circulation, *J. Phys. Oceanogr*., *10*, 1010–1031, 1980.

Illari, L., and J. C. Marshall, On the interpretation of eddy fluxes during a blocking episode, *J. Atmos. Sci*., *40*, 2232–2242, 1983.

Kamenkovich, I. V., and J. Pedlosky, Radiating instability of nonzonal ocean currents, *J. Phys. Oceanogr*., *26*, 622–643, 1996.

Kamenkovich, I. V., and J. Pedlosky, Radiation of energy from nonzonal ocean currents: Nonlinear regime, I, Single wave development, *J. Phys. Oceanogr*., *28*, 1661–1682, 1998.

Krauss, W., The North Atlantic Current, *J. Geophys. Res*., *91*, 5061–5074, 1986.

Levitus, S., R. Burgett, and T. P. Boyer, *World Ocean Atlas 1994*, vol. 3, *Salinity*, 99 pp., U.S. Dept. of Comm., Washington, D. C., 1994.

Lozier, M. S., Evidence for large-scale eddy-driven gyres in the North Atlantic, *Science*, *277*, 361–354, 1997.

Malanotte-Rizzoli, P., D. G. Haidvogel, and R. E. Young, Numerical solution of transient boundary-forced radiation, I, The linear regime, *J. Phys. Oceanogr*., *17*, 1439–1457, 1987.

Malanotte-Rizzoli, P., N. G. Hogg, and R. E. Young, Stochastic wave radiation by the Gulf Stream: Numerical experiments, *Deep Sea Res*., *Part I*, *42*, 389–423, 1995.

Nakamura, H., M. Nakamura, and J. L. Anderson, The role of high- and low-frequency dynamics in blocking formation, *Mon. Weather Rev*., *125*, 2074–2093, 1997.

Nakamura, M., On modified rotational and divergent eddy fluxes and their application to blocking diagnoses, *Q. J. R. Meteorol. Soc*., *124*, 341–352, 1998.

Oort, A. H., and J. P. Peixoto, Global angular momentum and energy balance requirements from observations, *Adv. Geophys*., *25*, 355–490, 1983.

Owens, W. B., A statistical description of the mean circulation and eddy variability in the northwestern Atlantic using SOFAR floats, *Prog. Oceanogr*., *28*, 257–303, 1991.

Pedlosky, J., On the radiation of mesoscale energy in the mid-ocean, *Deep Sea Res*., *24*, 591–600, 1977.

Pickart, R. S., and W. M. Smethie Jr., How does the deep western boundary current cross the Gulf Stream?, *J. Phys. Oceanogr*., *23*, 2602–2616, 1993.

Plumb, R. A., On the three-dimensional propagation of stationary waves, *J. Atmos. Sci*., *42*, 217–229, 1985.

Plumb, R. A., Three-dimensional propagation of transient quasi-geostrophic eddies and its relationship with the eddy forcing of the time-mean flow, *J. Atmos. Sci*., *43*, 1657–1678, 1986.

Rhines, P. B., and W. R. Holland, A theoretical discussion of eddy-driven mean flows, *Dyn. Atmos. Oceans*, *3*, 289–325, 1979.

Rhines, P. B., and W. R. Young, A theory of wind-driven ocean circulation, I, Mid-ocean gyres, *J. Mar. Res*., *40*, Suppl., 559–596, 1982a.

Rhines, P. B., and W. R. Young, Homogenization of potential vorticity in planetary gyres, *J. Fluid Mech*., *122*, 347–368, 1982b.

Richardson, P. L., A census of eddies observed in North Atlantic SOFAR float data, *Prog. Oceanogr*., *31*, 1–50, 1993.

Schmitz, W. J., Jr., and J. D. Thompson, On the effects of horizontal resolution in a limited-area model of the Gulf Stream system, *J. Phys. Oceanogr*., *23*, 1001–1007, 1993.

Schmitz, W. J., Jr., W. R. Holland, and J. F. Price, Mid-latitude mesoscale variability, *Rev. Geophys*., *21*, 1109–1119, 1983.

Semtner, A. J., and R. M. Chervin, Ocean general circulation from a global eddy-resolving model, *J. Geophys. Res*., *97*, 5493–5550, 1992.

Shutts, G. J., The propagation of eddies in diffluent jetstreams: Eddy vorticity forcing of "blocking" flow fields, *Q. J. R. Meteorol. Soc*., *109*, 737–761, 1983.

Smith, R. D., J. K. Dukowicz, and R. C. Malone, Parallel ocean general circulation modeling, *Physica D*, *60*, 38–61, 1992.

Spall, M. A., Mechanism for low-frequency variability and salt flux in the Mediterranean salt tongue, *J. Geophys. Res*., *99*, 10,121–10,129, 1994.

Spall, M. A., Dynamics of the Gulf Stream/Deep Western Boundary Current crossover, I, Entrainment and recirculation, *J. Phys. Oceanogr*., *26*, 2152–2168, 1996a.

Spall, M. A., Dynamics of the Gulf Stream/Deep Western Boundary Current crossover, II, Low-frequency internal oscillations, *J. Phys. Oceanogr*., *26*, 2169–2182, 1996b.

Thompson, J. D., and W. J. Schmitz Jr., A limited-area model of the Gulf Stream: Design, initial experiments, and model/data intercomparison, *J. Phys. Oceanogr*., *19*, 791–814, 1989.

Watts, D. R., K. L. Tracey, J. M. Bane, and T. J. Shay, Gulf Stream path and thermocline structure near 74°W and 68°W, *J. Geophys. Res*., *100*, 18,291–18,312, 1995.

Wunsch, C. L., Western North Atlantic interior, in *Eddies in Marine Science*, edited by A. R. Robinson, pp. 46–65, Springer-Verlag, New York, 1983.

Wyrtki, K., L. Magaard, and J. Hager, Eddy energy in the oceans, *J. Geophys. Res*., *81*, 2641–2646, 1976.

Y. Chao and M. Nakamura, Jet Propulsion Laboratory, Mail Stop 300-323, 4800 Oak Grove Drive, Pasadena, CA 91109. (moto@pacific.jpl.nasa.gov)

(Received January 11, 1999; revised January 18, 2000; accepted January 18, 2000.)